10.3 –

Dynamical Integrity: Interpreting and Predicting Experimental Response

Giuseppe Rega

Department of Structural and Geotechnical Engineering
Sapienza University of Rome, Italy
Giuseppe.Rega@uniroma1.it

Coworkers: S. Lenci, M. Brocchini, M. Younis, L. Ruzziconi

DAY	TIME	LECTURE
Monday 05/11	14.00 -14.45	Historical Framework - A Global Dynamics Perspective in the Nonlinear Analysis of Systems/Structures
	15.00 -15.45	Achieving Load Carrying Capacity: Theoretical and Practical Stability
	16.00 -16.45	Dynamical Integrity: Concepts and Tools_1
Wednesday 07/11	14.00 -14.45	Dynamical Integrity: Concepts and Tools_2
	15.00 -15.45	Global Dynamics of Engineering Systems
	16.00 -16.45	**Dynamical integrity: Interpreting/Predicting Experimental Response**
Monday 12/11	14.00 -14.45	Techniques for Control of Chaos
	15.00 -15.45	A Unified Framework for Controlling Global Dynamics
	16.00 -16.45	Response of Uncontrolled/Controlled Systems in Macro- and Micro-mechanics
Wednesday 14/11	14.00 -14.45	A Noncontact AFM: (a) Nonlinear Dynamics and Feedback Control (b) Global Effects of a Locally-tailored Control
	15.00 -15.45	Exploiting Global Dynamics to Control AFM Robustness
	16.00 -16.45	Dynamical Integrity as a Novel Paradigm for Safe/Aware Design

Motivations (1)

☑ theoretical work

concept, definitions,
safe basins, integrity measures

☑ numerical work

analyses of the dynamics of various mechanical systems and model by extensive numerical simulations

☐ experimental work?

is dynamical integrity also useful in experiments?

can it help in explaining some ‘strange’ behaviour?

Motivations (2)

mechanical model

equations of motion

dynamical integrity analysis

predicted robust (not only stable) response

experiments

parametric experimental analsys

observed response

?

Contents

In other words, the key point is:

Can we use dynamical integrity to interpret experimental results?

Yes, we can

1) **A macro-example: Rotating pendulum**
2) **A micro-example: MEMS**

Background: The parametrically excited pendulum (1)

$$\ddot{x} + 0.1\dot{x} + [1 + p\cos(2t)]\sin(x) = 0$$

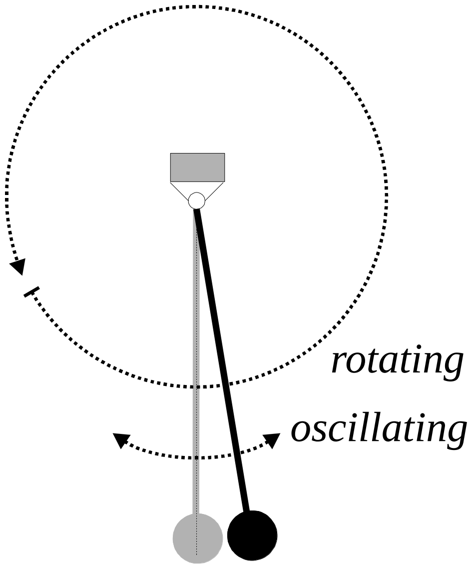

- "an antique but evergreen physical model" [Butikov]
- competing in-well attractors (oscillations) and out-of-well attractors (rotations)
- theoretical, experimental and numerical studies

Background: The parametrically excited pendulum (2)

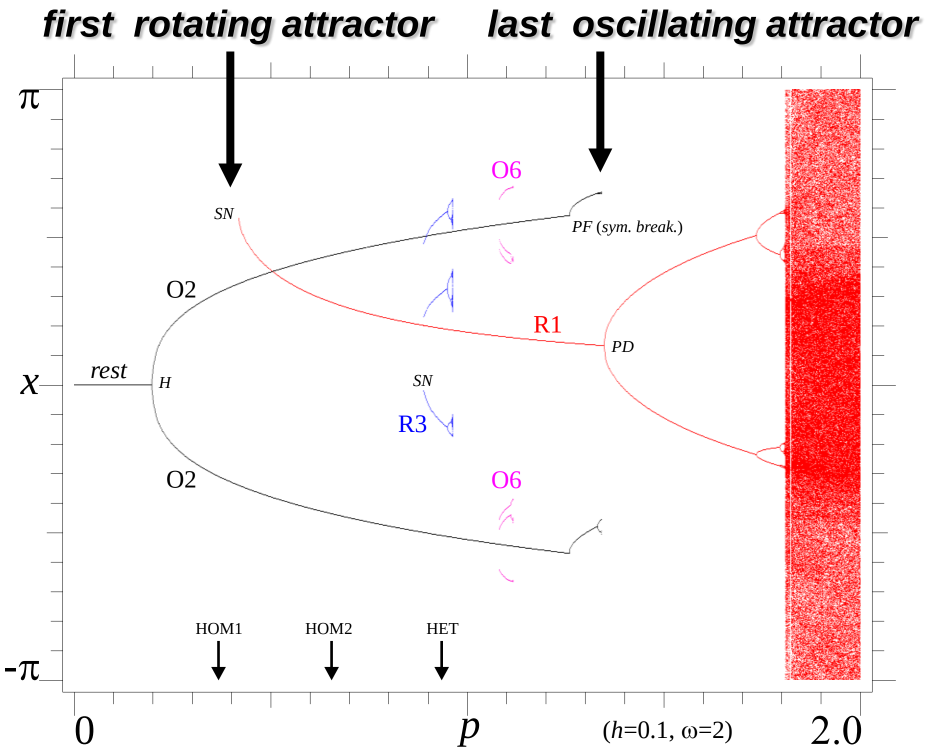

p	event	comment
0.196	H	the rest position loses stability. O2 appears
0.367	HOM1	homoclinic bifurcation of HS
0.418	SN	R1 appear through a SN bifurcation
0.655	HOM2	homoclinic bifurcation of DR1
0.888	SN	R3 appear through a SN bifurcation
0.935	HET	heteroclinic bifurcation of DR1 and Ir
0.948	PD	R3 undergo a PD bifurcation followed by a PD cascade
0.961	CR	the PD cascade of R3 ends by a CR. R3 disappear
1.082	SN	O6 appears through a SN bifurcation
1.111	PF	O6 undergoes a PF bifurcation, and two oscillating solutions of period 6, still named O6, appear
1.116	PD	O6 undergo a PD bifurcation followed by a PD cascade
1.118	CR	the PD cascade of O6 ends by a CR. O6 disappear
1.260	PF	O2 undergoes a PF bifurcation, and two oscillating solutions of period 2, still named O2, appear
1.332	PD	O2 undergo a PD bifurcation followed by a PD cascade
1.342	CR	the PD cascade of O2 ends by a CR. O2 disappear
1.349	PD	R1 undergo a PD bifurcation followed by a PD cascade
1.809	CR	the PD cascade of R1 ends by a CR. R1 disappear, and tumbling chaos becomes the unique attractor

<u>attractors</u>

O2	main oscillating solution of period 2
R1	main rotating solutions of period 1
R3	secondary rotating solutions of period 3
O6	secondary oscillating solution of period 6

<u>main saddles</u>

HS	hilltop saddles
DR1	direct saddles born at the SN bifurcation where R1 appear
IR1	inverse saddles after the PD bifurcation of R1
Ir	inverse saddle replacing the rest position at the H bifurcation

<u>bifurcations</u>

SN	saddle-node
PD	period-doubling
PF	pitchfork (or symmetry breaking)
H	Hopf
CR	crisis
HOM/HET	homoclinic/heteroclinic

- Four main competing attractors (oscillating and rotating: O2, R1, O6, R3)
- ω=2 (parametric resonance)

An example of basins of attraction

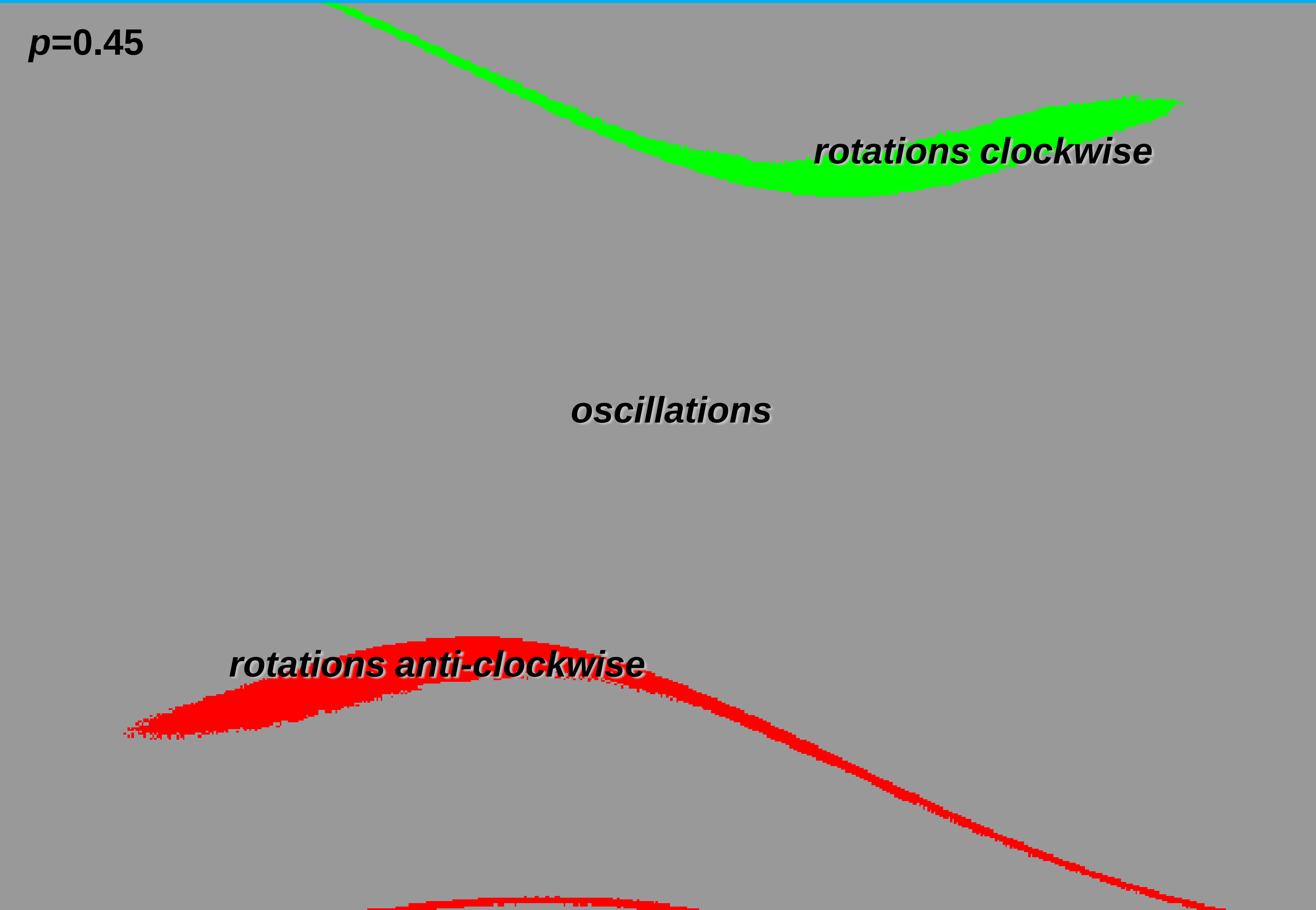

The wave flume at UNIVPM

- Length 50 [m], width 1 [m], height 1.3 [m]
- HR Wallingford waves generator, mono-chromatic and colored waves
- Maximum level of water 1 [m]
- Waves frequencies from 0.04 to 2 [Hz]
- Waves amplitudes about 5÷10 [cm]

The pendulum (1)

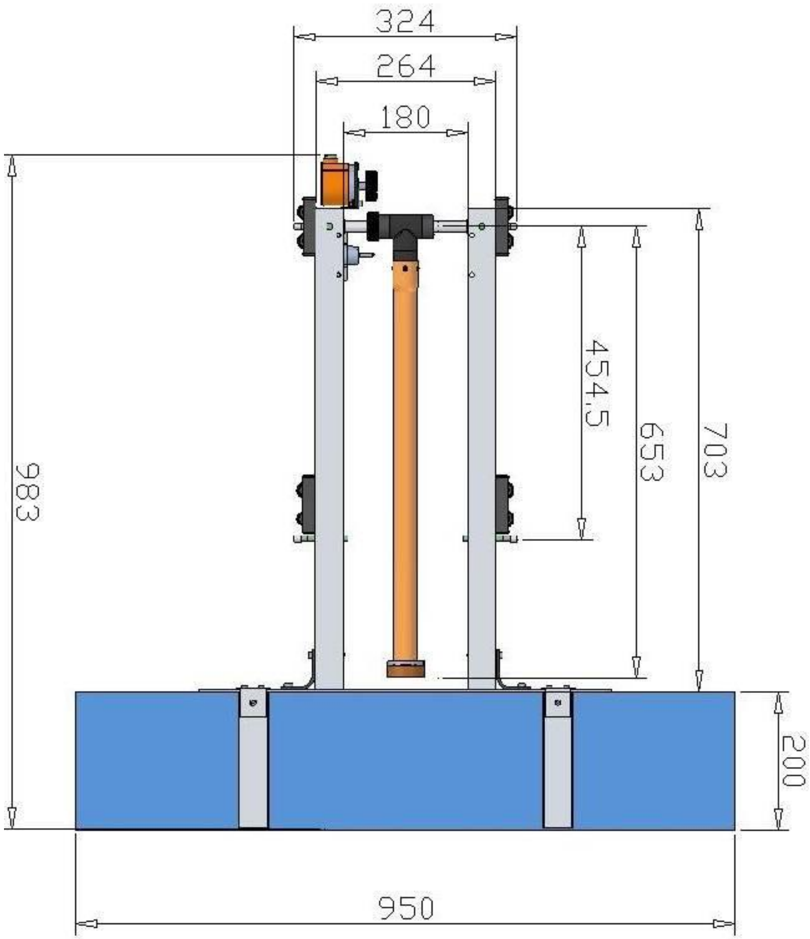

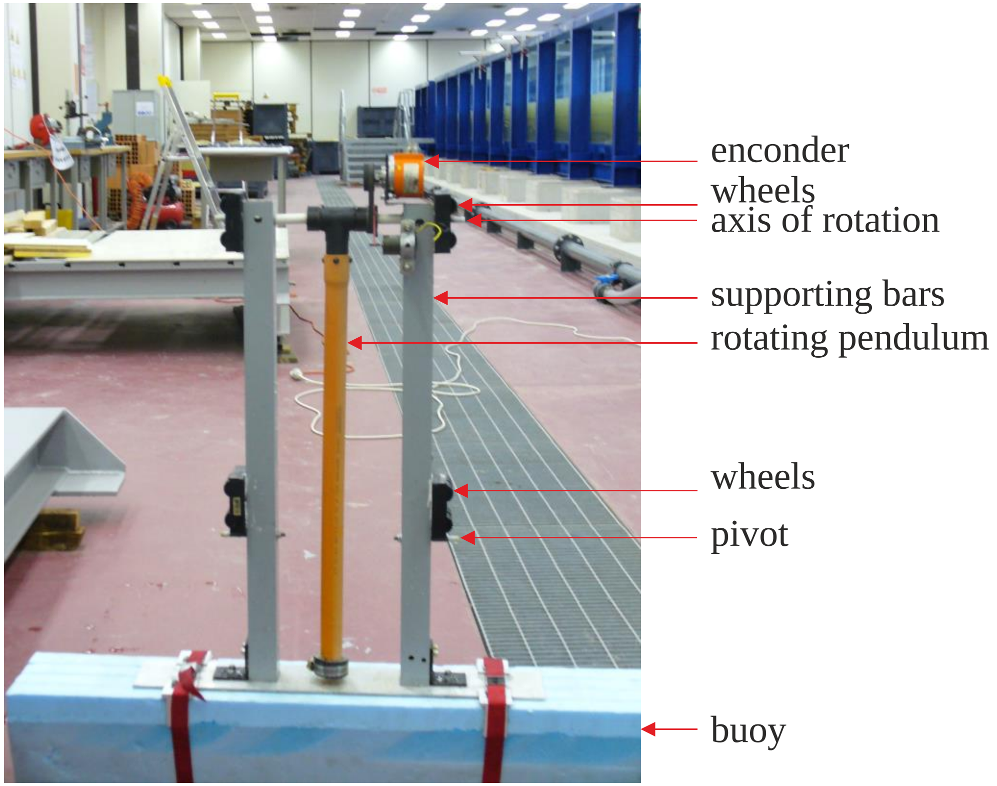

- Total weight about 8 Kg

The pendulum (2)

- PVC bar, mass of 0.23 Kg, with an added steel mass of 0.3 Kg at the end of the bar
- l=586 [mm] $\rightarrow$ ω_0=4.09 and f_0=0.65 [Hz]. Experiments above and below the parametric resonance f=2f_0=1.3 [Hz]
- Buoy made of polyurethane, 950×200×160 [mm^3]
- Damping coefficient h=0.015 (exper. determined)

$$\ddot{\theta} + h\dot{\theta} + (1 + \ddot{y}_0)\sin\theta = 0$$

The experimental rig

First of all, an experimental rotation

- Rotations have small basins with respect to competing oscillations, so they are difficult to be detected experimentally

A representative time history, f=1.2 [Hz]

Pivot vertical displacement

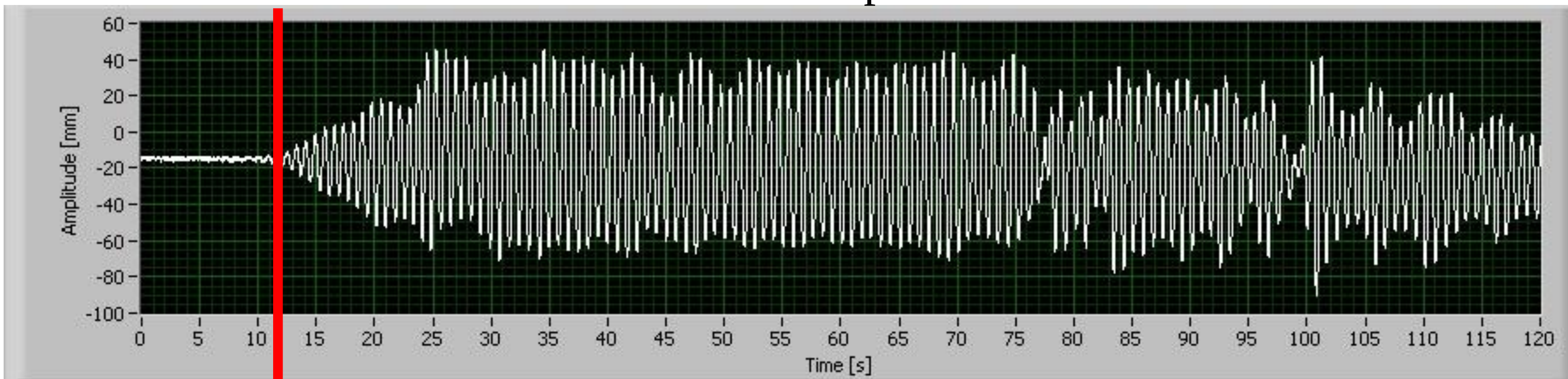

Angular velocity of the pendulum

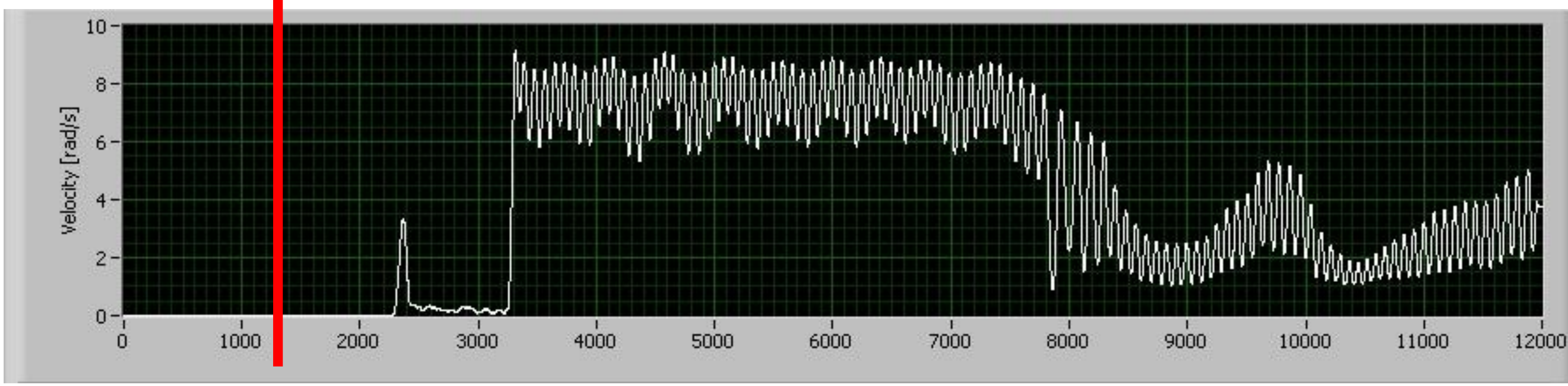

The first travelling wave produced by the generator arrives at the buoy

A representative time history, f=1.2 [Hz]

Pivot vertical displacement

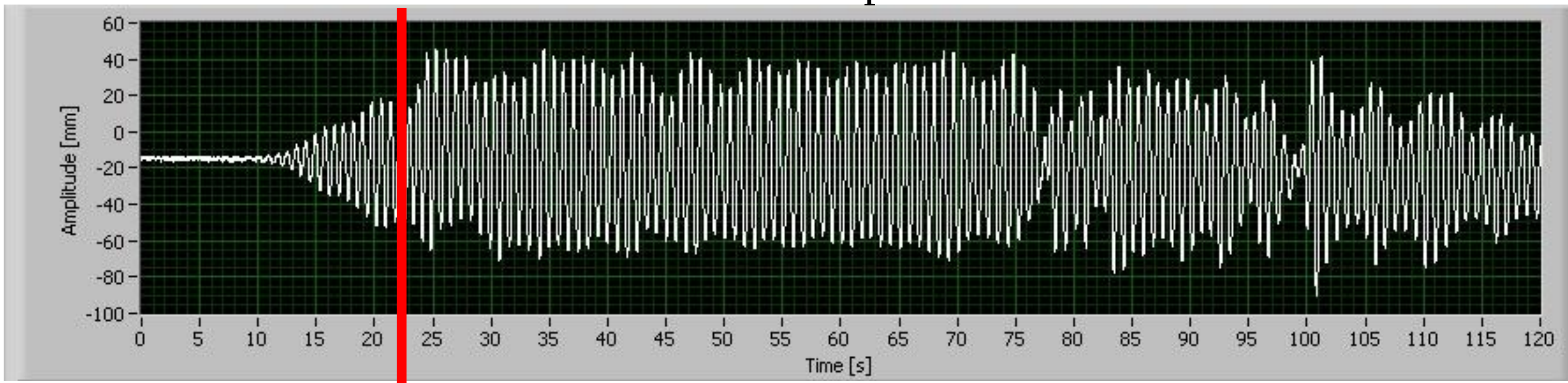

Angular velocity of the pendulum

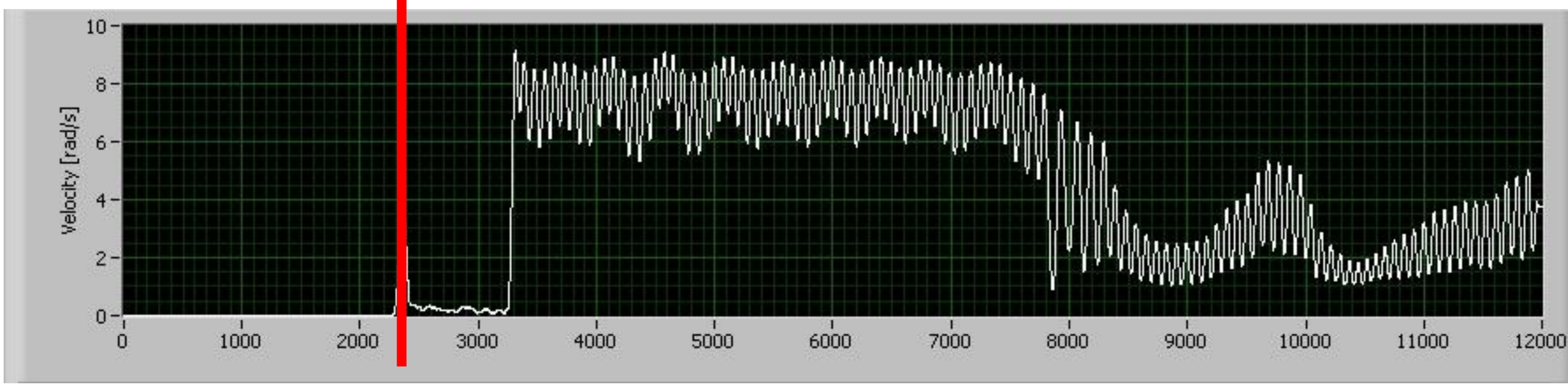

During the transient the operator brings the pendulum to the initial position

A representative time history, f=1.2 [Hz]

Pivot vertical displacement

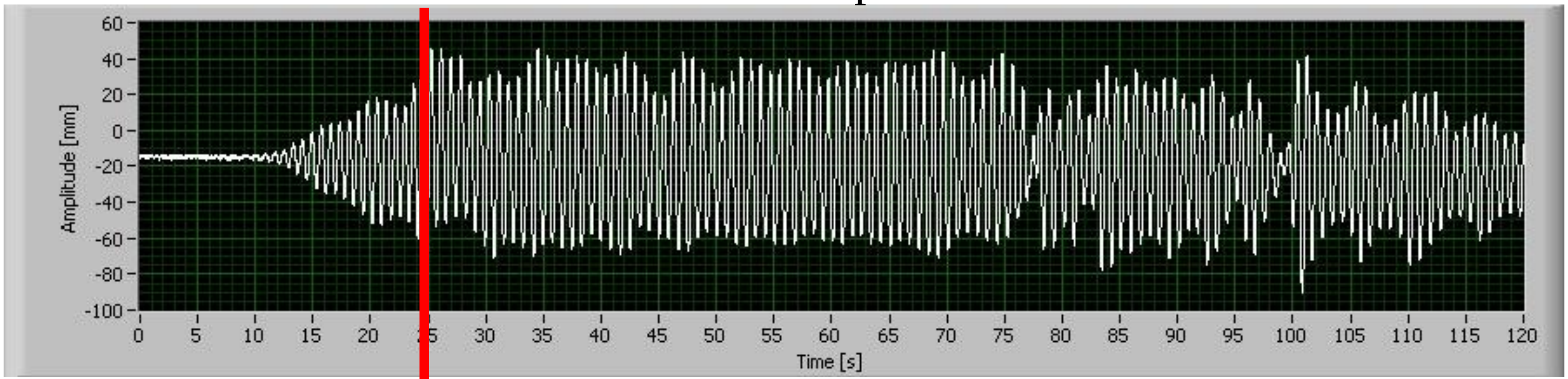

Angular velocity of the pendulum

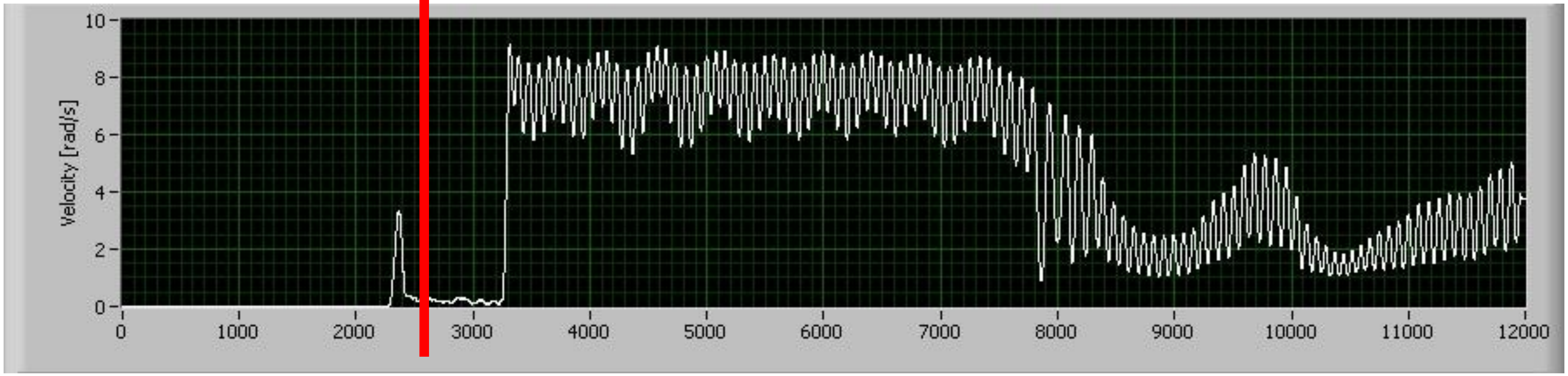

End of transient. From now on steady state waves support the buoy

A representative time history, f=1.2 [Hz]

Pivot vertical displacement

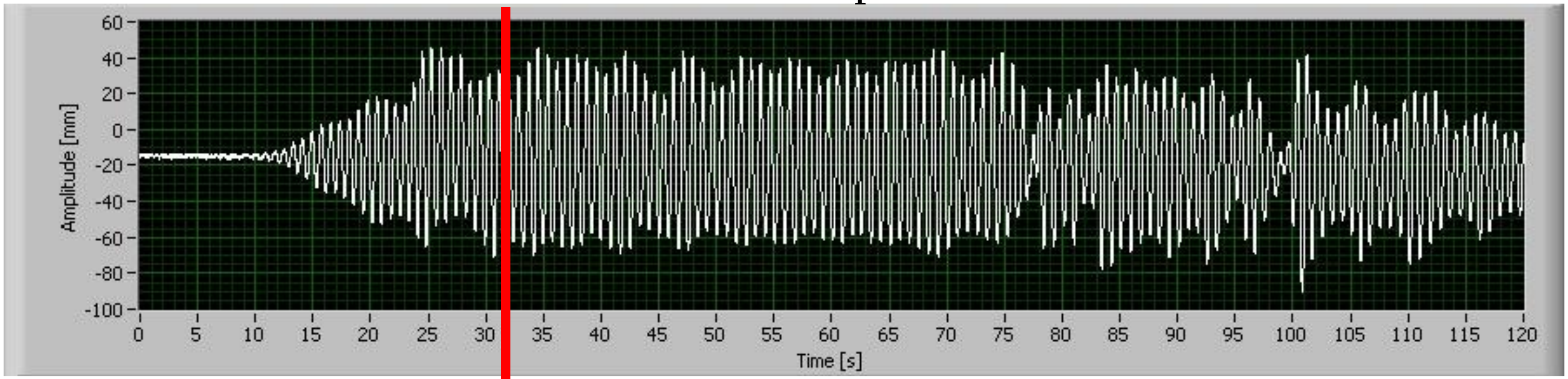

Angular velocity of the pendulum

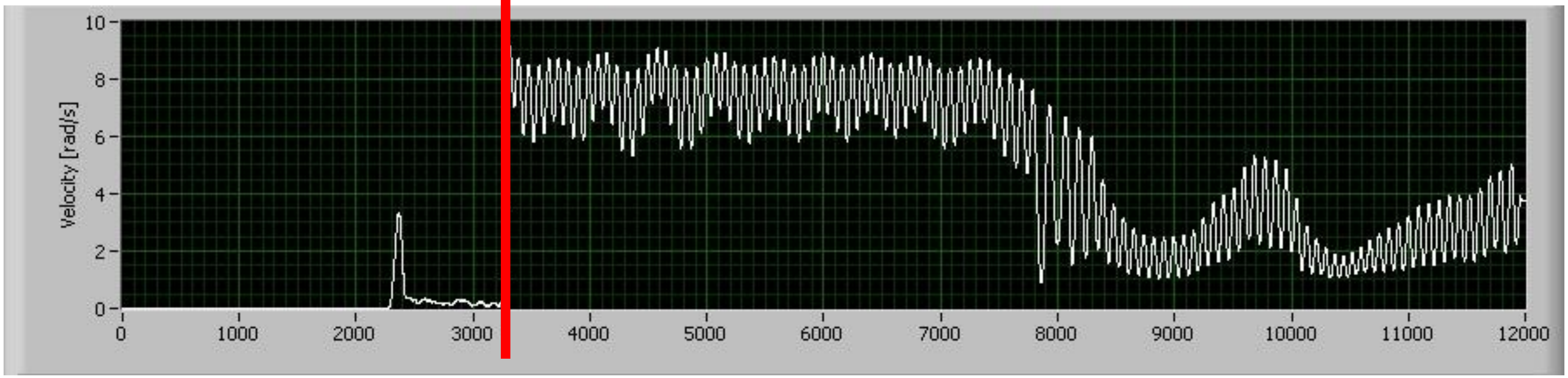

Pendulum starts rotations

A representative time history, f=1.2 [Hz]

Pivot vertical displacement

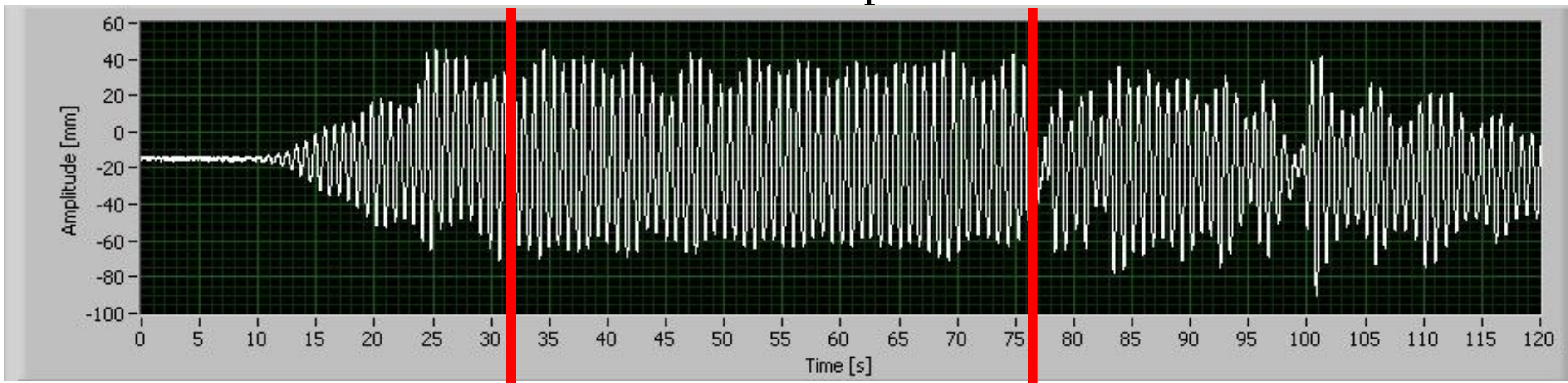

Angular velocity of the pendulum

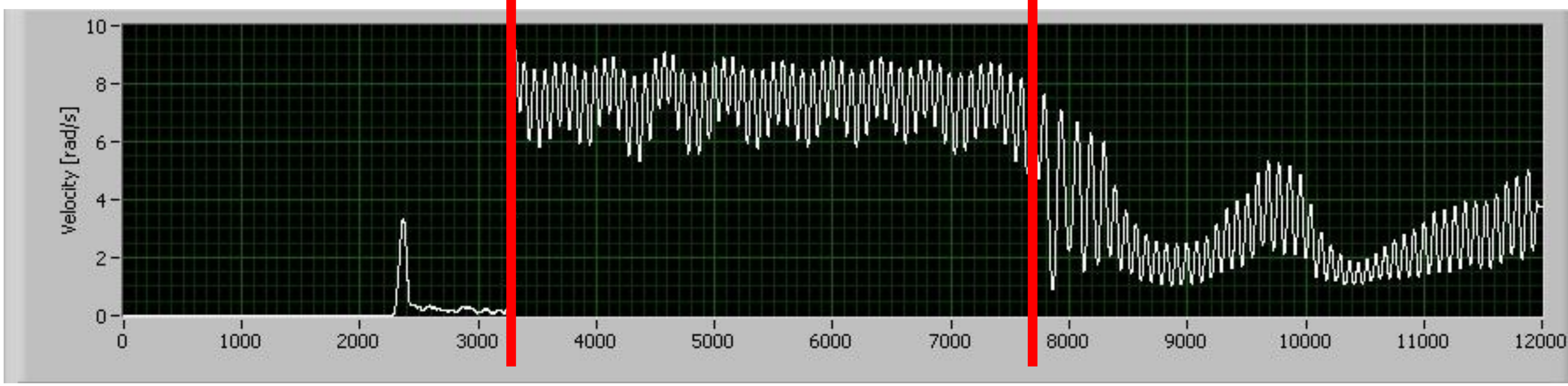

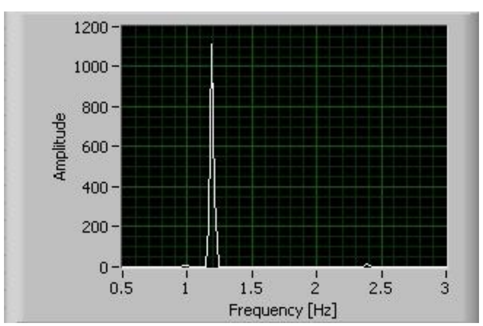

FFT → Regular rotation, 40 [sec]

A representative time history, f=1.2 [Hz]

Pivot vertical displacement

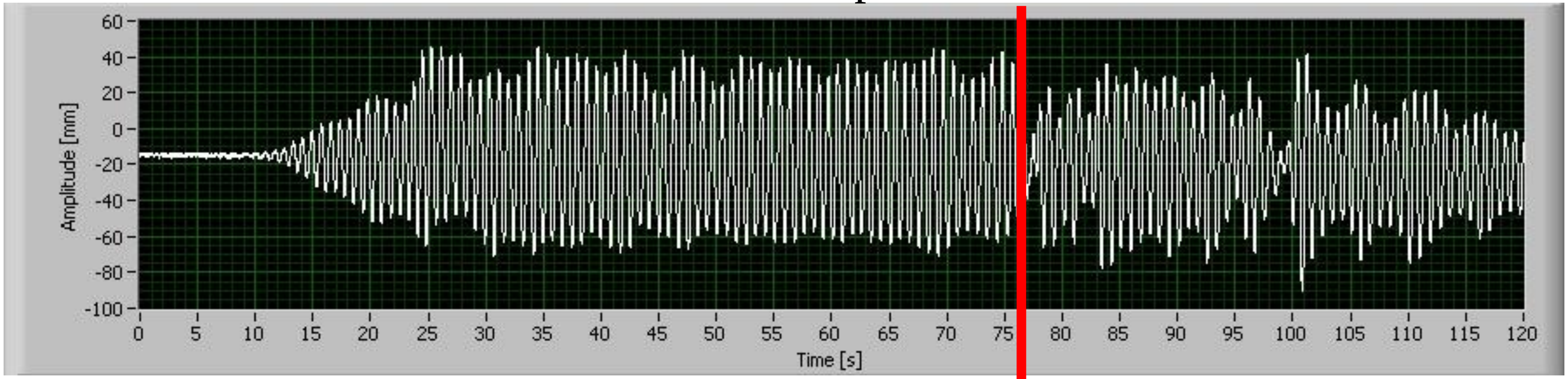

Angular velocity of the pendulum

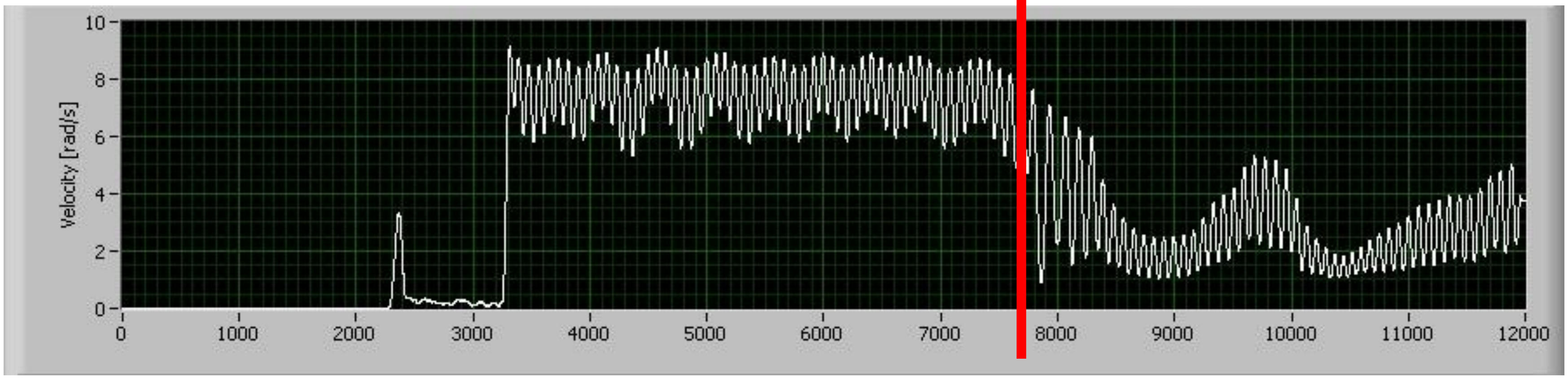

Reflected waves arrive at the buoy and destroy the regular rotation

Theoretical behaviour for increasing amplitude

- Generic features: SN (appearance) → PD → PD cascade → BC (disappearance)

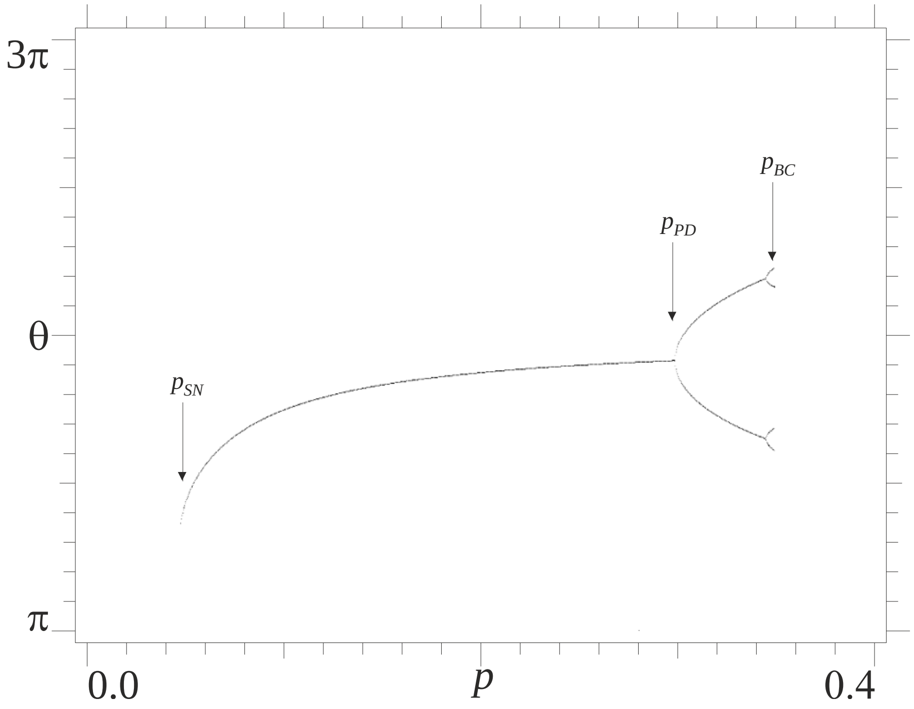

Behaviour chart – main experimental result

- Theoretical vs experimental

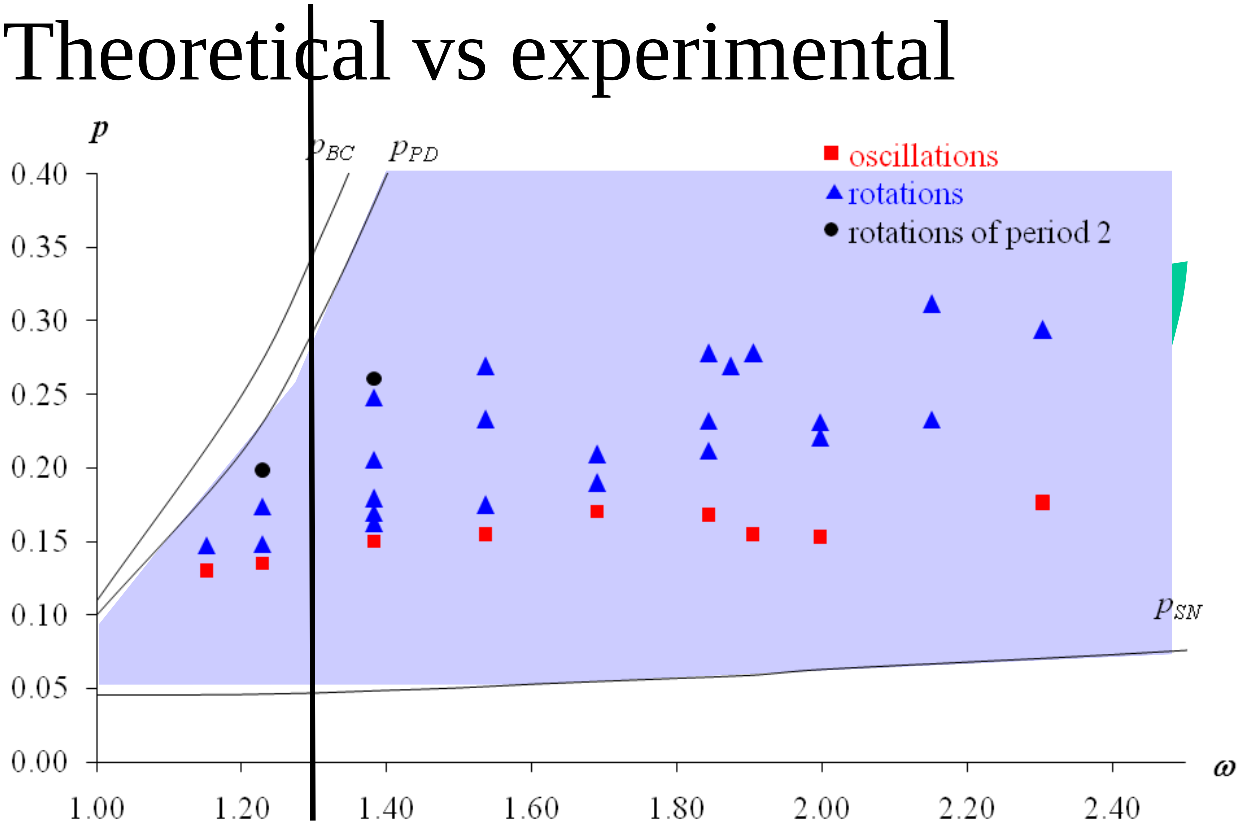

- PD captured experimentally
- Theory: rotations exist in a **large region**
- Experiments: rotations exist in a **narrow strip**

Theoretical vs experimental 'disagreement'

- Differences between theoretical and experimental regions of existence of rotations call for a justification
- Partially due to the experimental approximations, of course
- Even with a "perfect" experiment, we would never reproduce experimentally the whole region of existence, but only a (possibly larger) central strip $\longrightarrow$

robustness and **dynamical integrity** issues

Present dynamical integrity analysis

- Safe basins are basins of attraction of the clockwise rotation
- The integrity measure is the Integrity Factor (IF)
- Several integrity profiles built over the region of existence of rotations

A representative integrity profile, ω=1.3

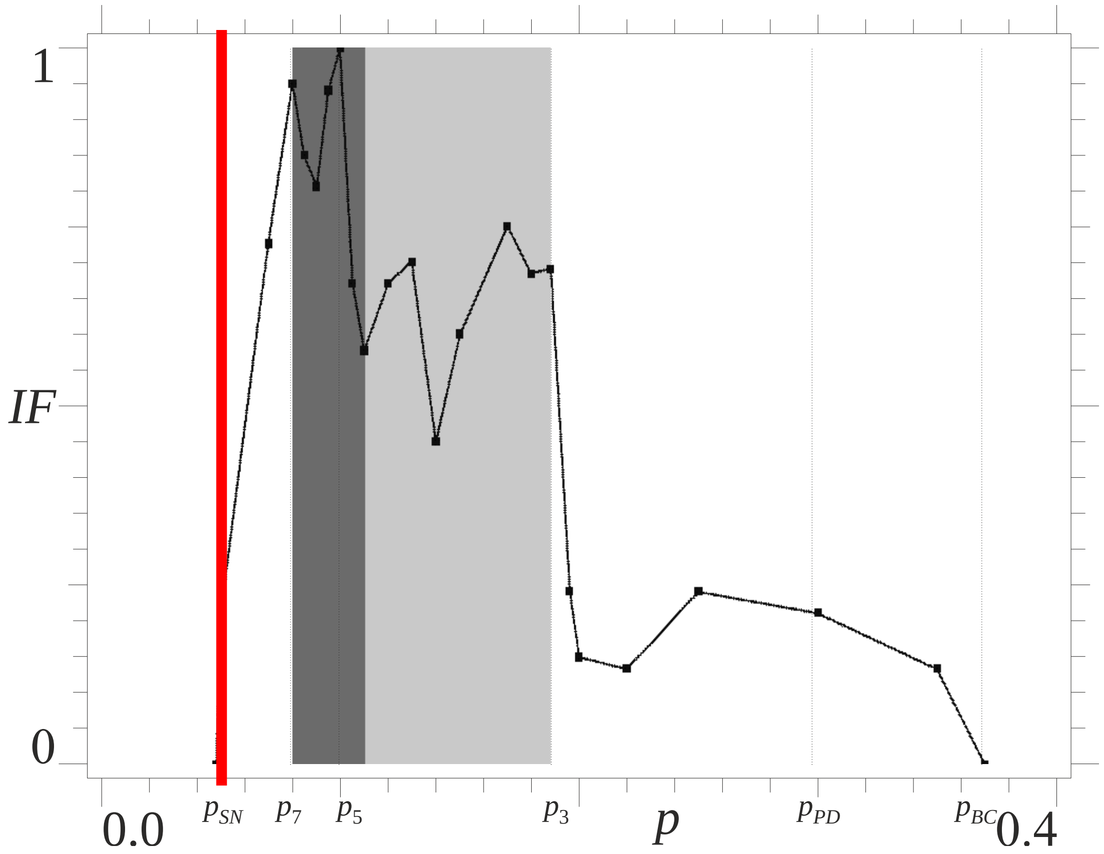

Main rotation appears through a saddle-node (SN) bifurcation.

Starting point of the integrity profile

A representative integrity profile, ω=1.3

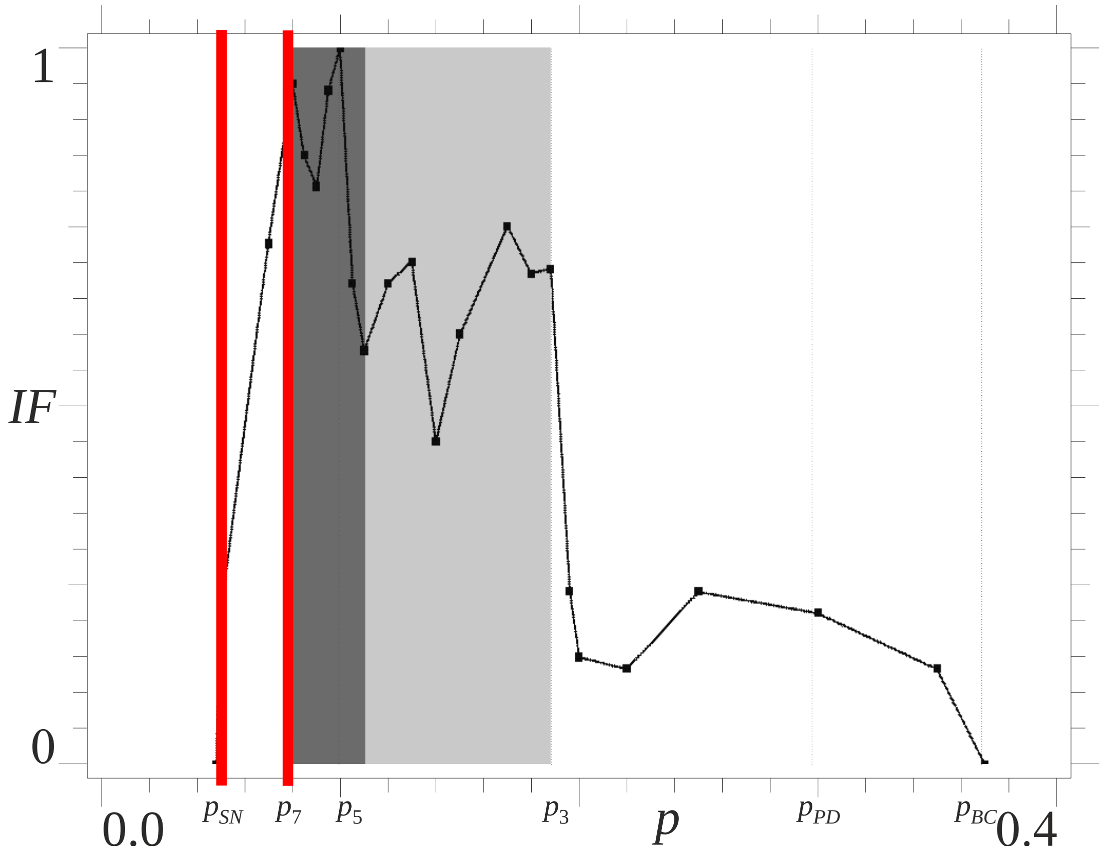

IF is increasing, but not yet large enough.

Rotations are not robust, cannot be observed in practice (indeed, as it happens !)

A representative integrity profile, ω=1.3

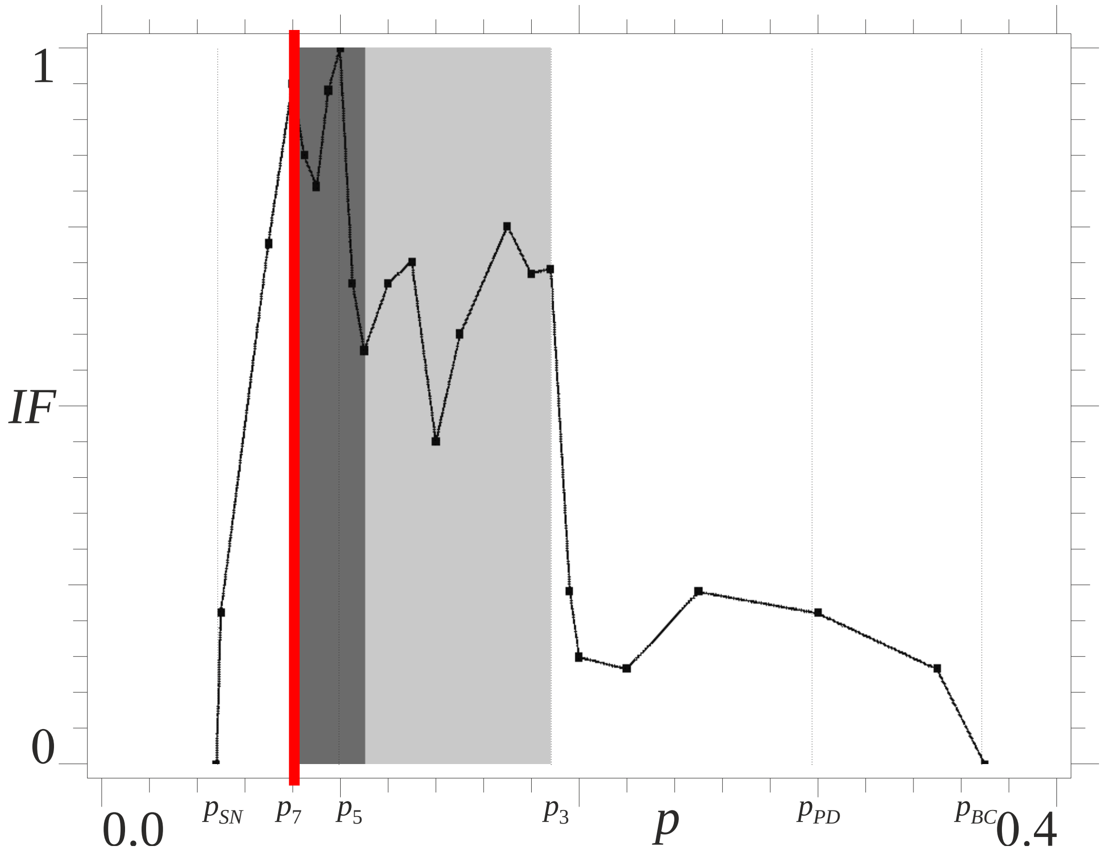

Rotation of period 7 appears by a SN inside the basin of attraction of the main rotation.

→ Instantaneous decrement of *IF*

A representative integrity profile, ω=1.3

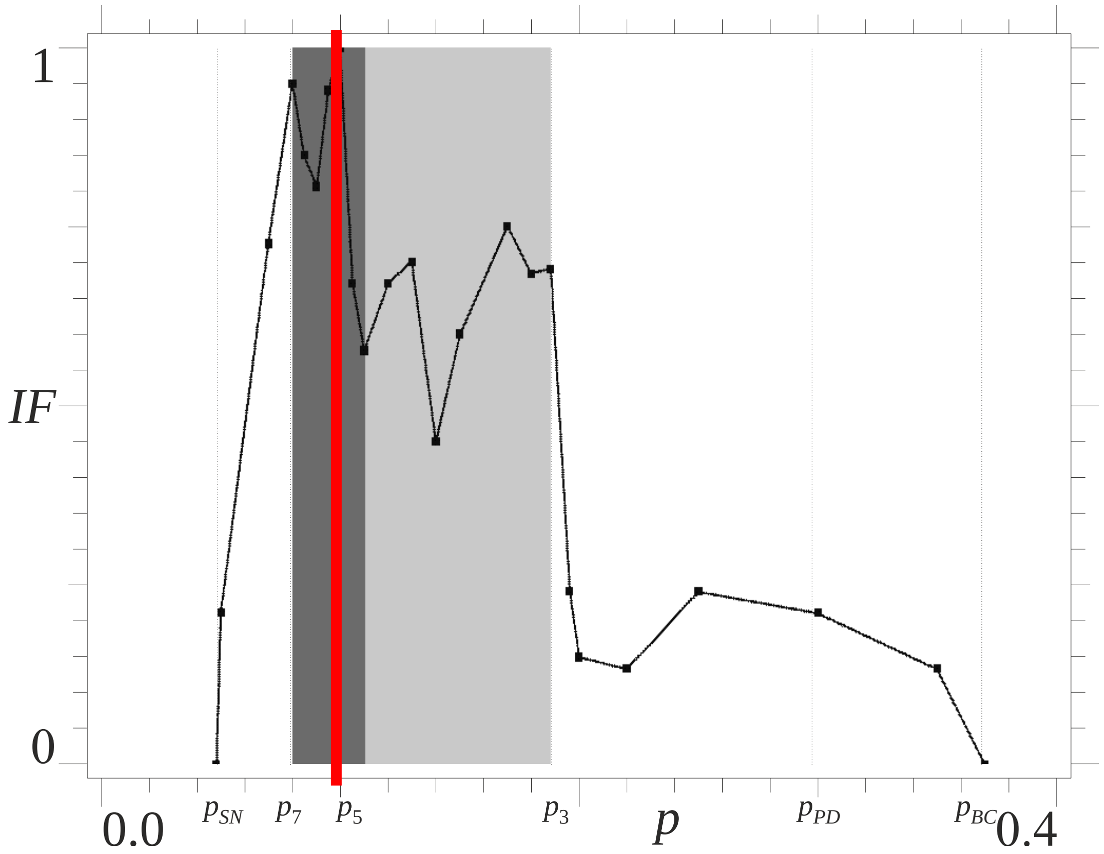

Rotation of period 5 appears by a SN inside the basin of attraction of the main rotation

→ Larger fall down of *IF* (R5 more robust than R7)

A representative integrity profile, ω=1.3

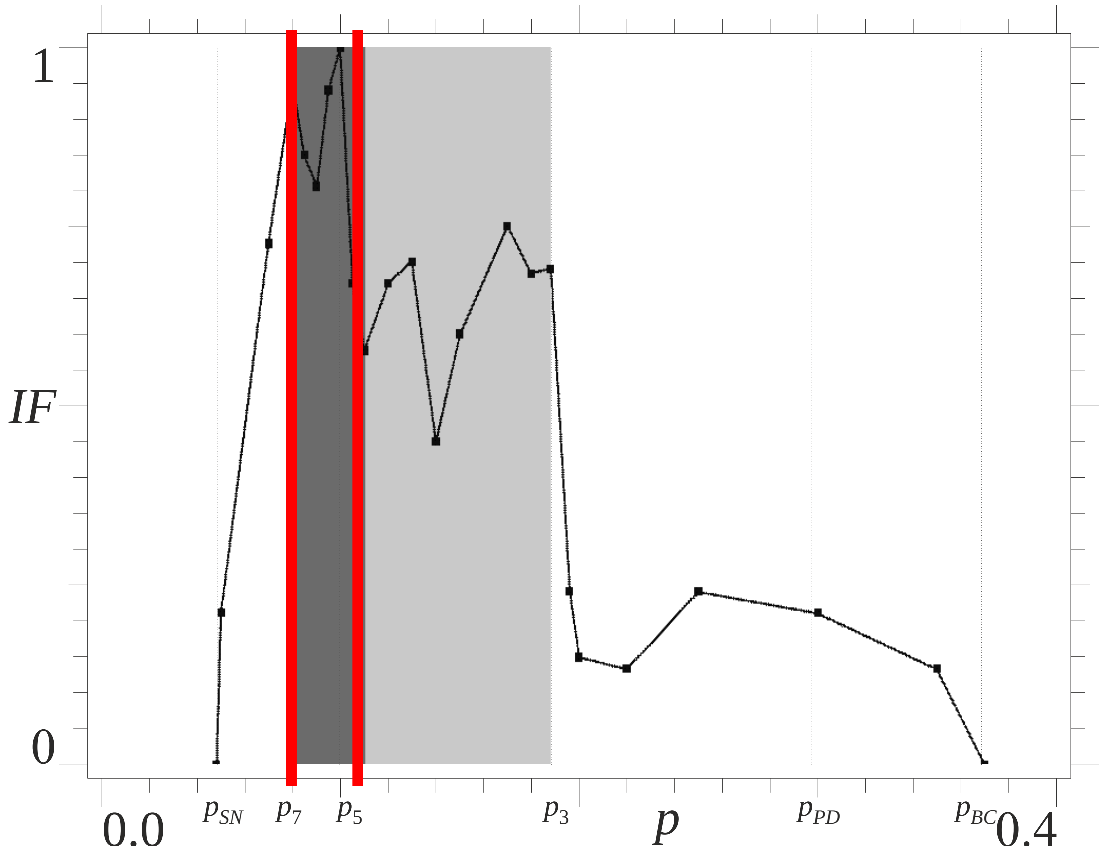

Region of largest IF, largest safety: here rotations are **robust** and **can be observed experimentally** (as it happens!)

A representative integrity profile, ω=1.3

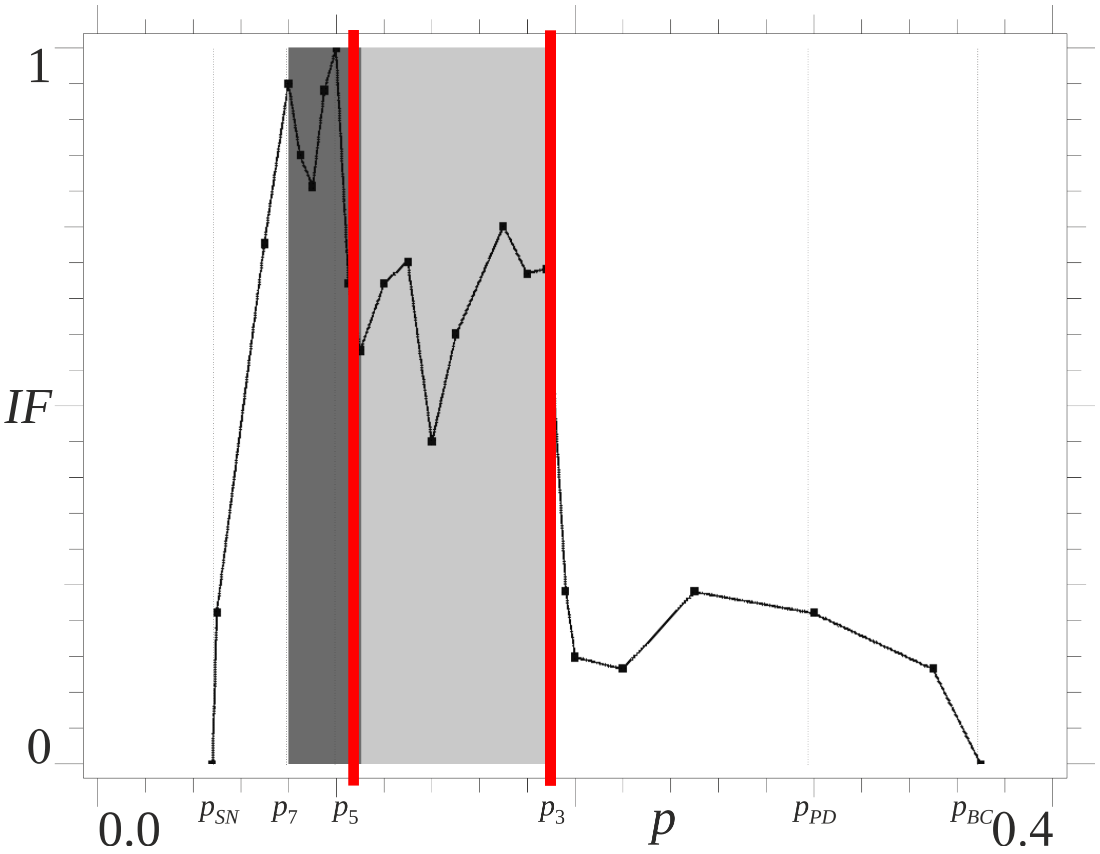

Region of large IF. Robustness decreased, but still large enough to observe experimental rotations (as happens!)

A representative integrity profile, ω=1.3

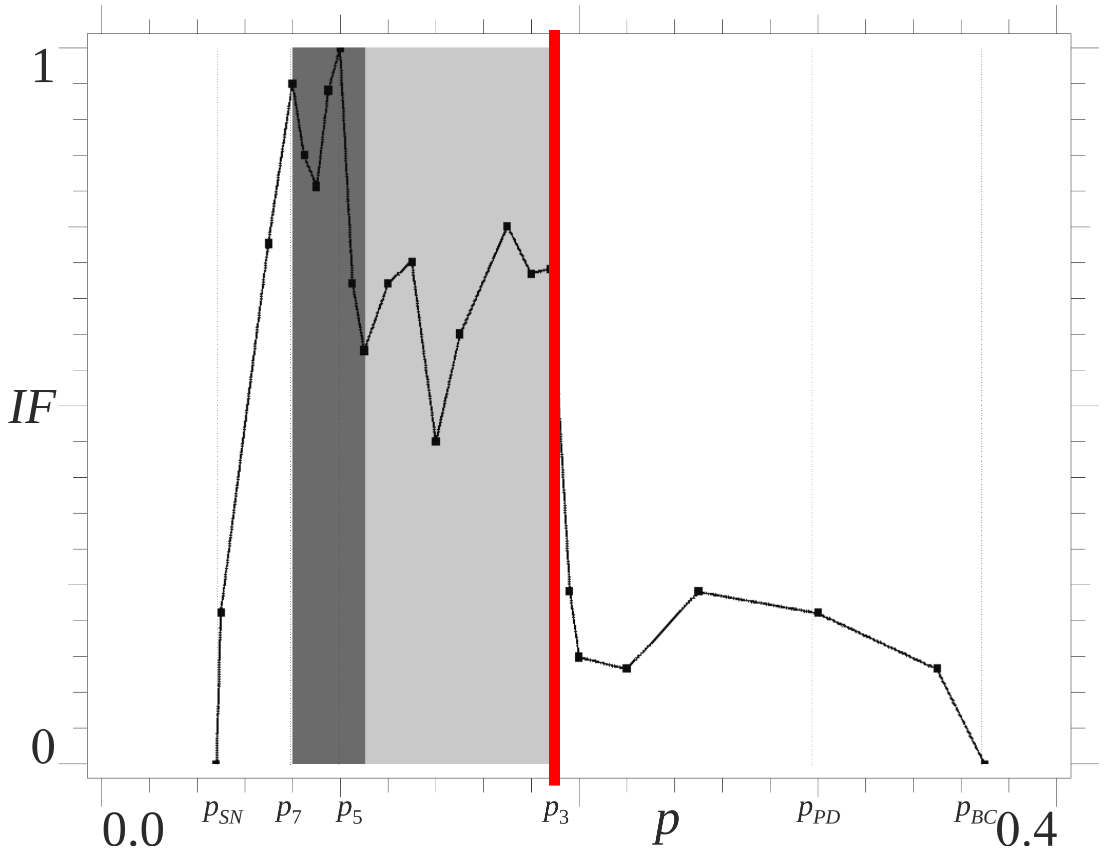

Rotation of period 3 appears by a SN inside the basin of attraction of the main rotation ⇒ Largest fall of *IF* (R3 more robust than R5, R7)

A representative integrity profile, ω=1.3

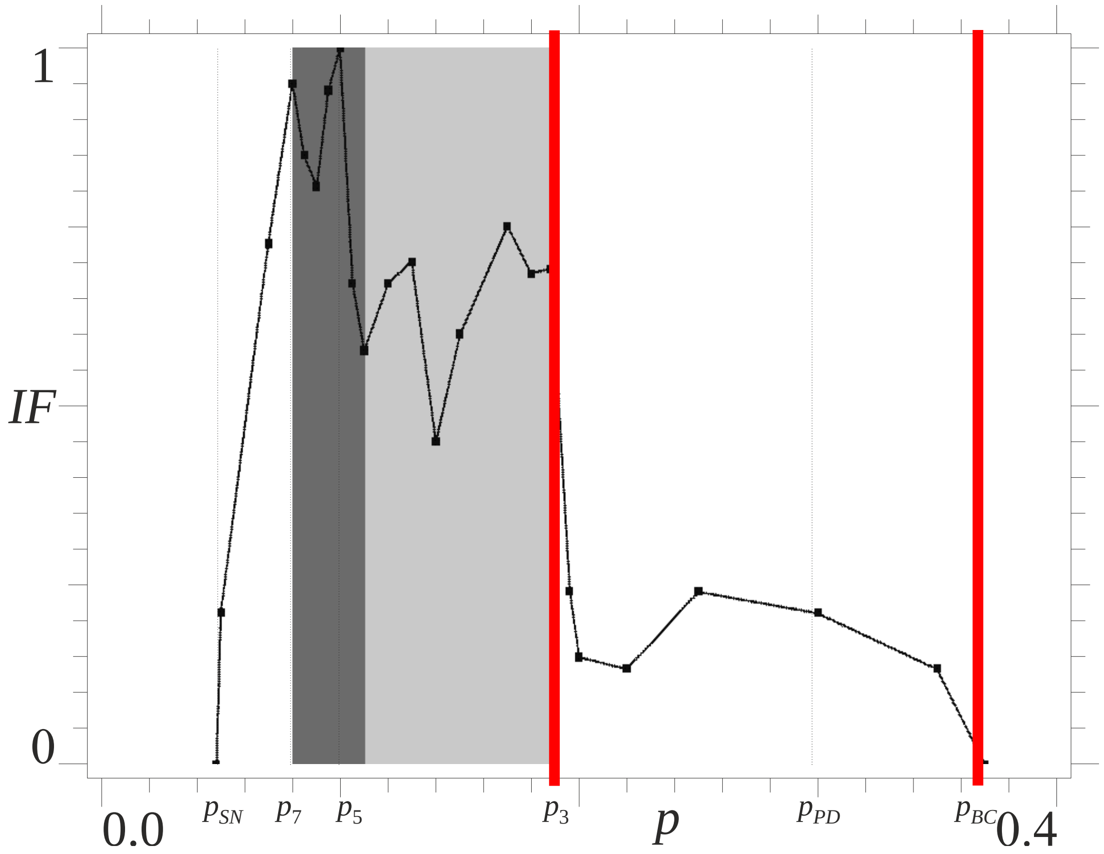

After the R3 fall, **IF** is **residual. No hope to observe experimental rotations** (as happens!)

A representative integrity profile, ω=1.3

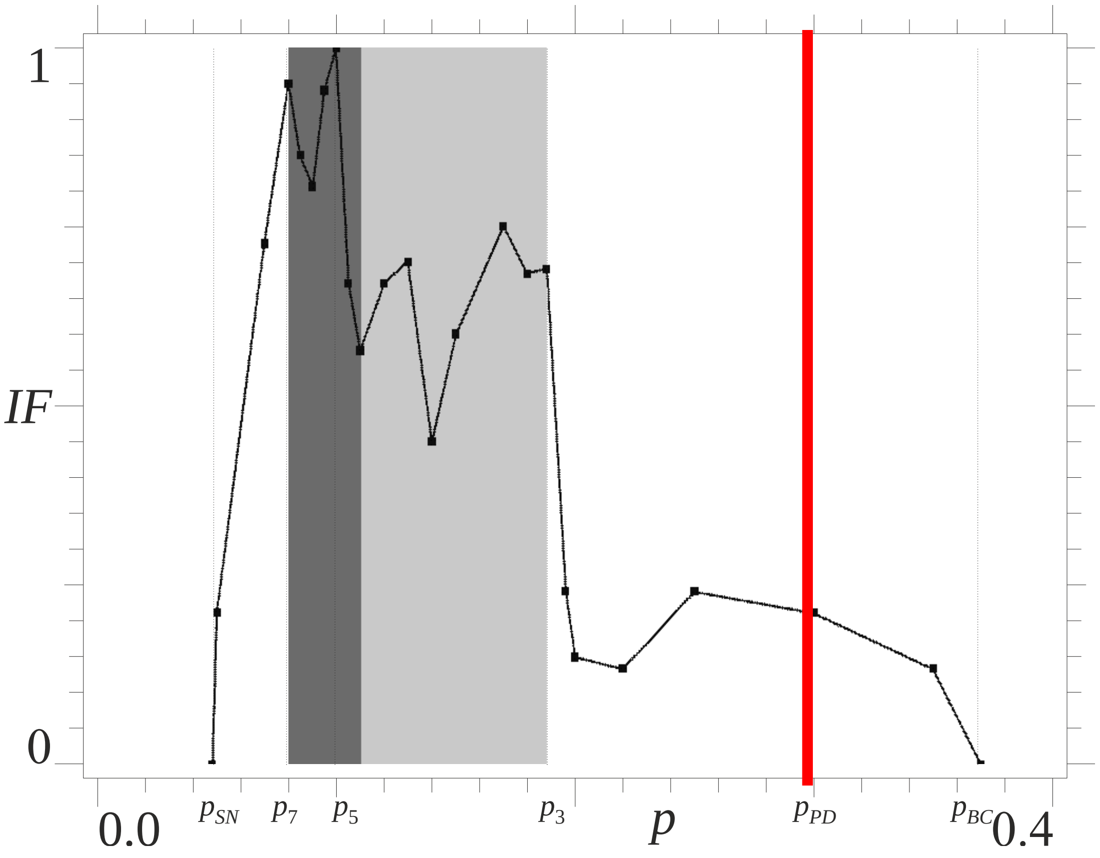

Period doubling bifurcation of the main rotation: no effects on integrity, indeed solely marginal

A representative integrity profile, ω=1.3

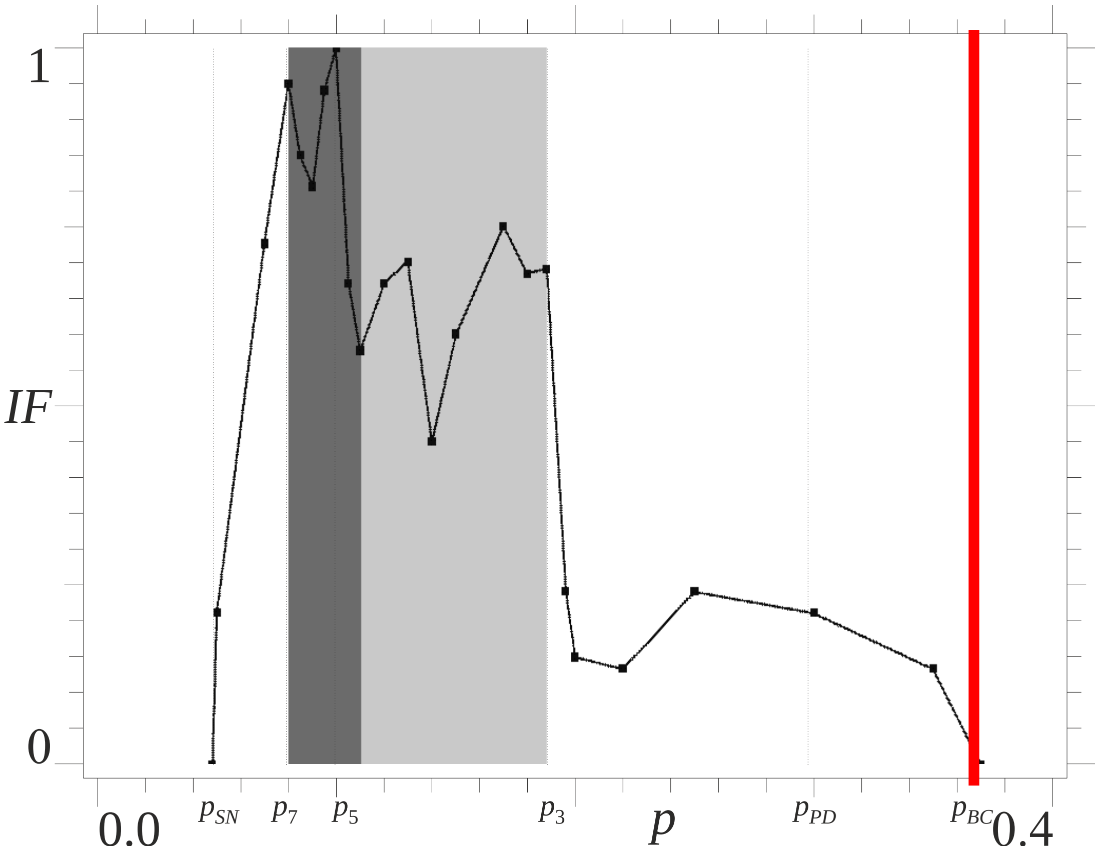

Disappearance of the attractor by a boundary crisis.

Ending point of the integrity profile

Theoretical justification of experimental results

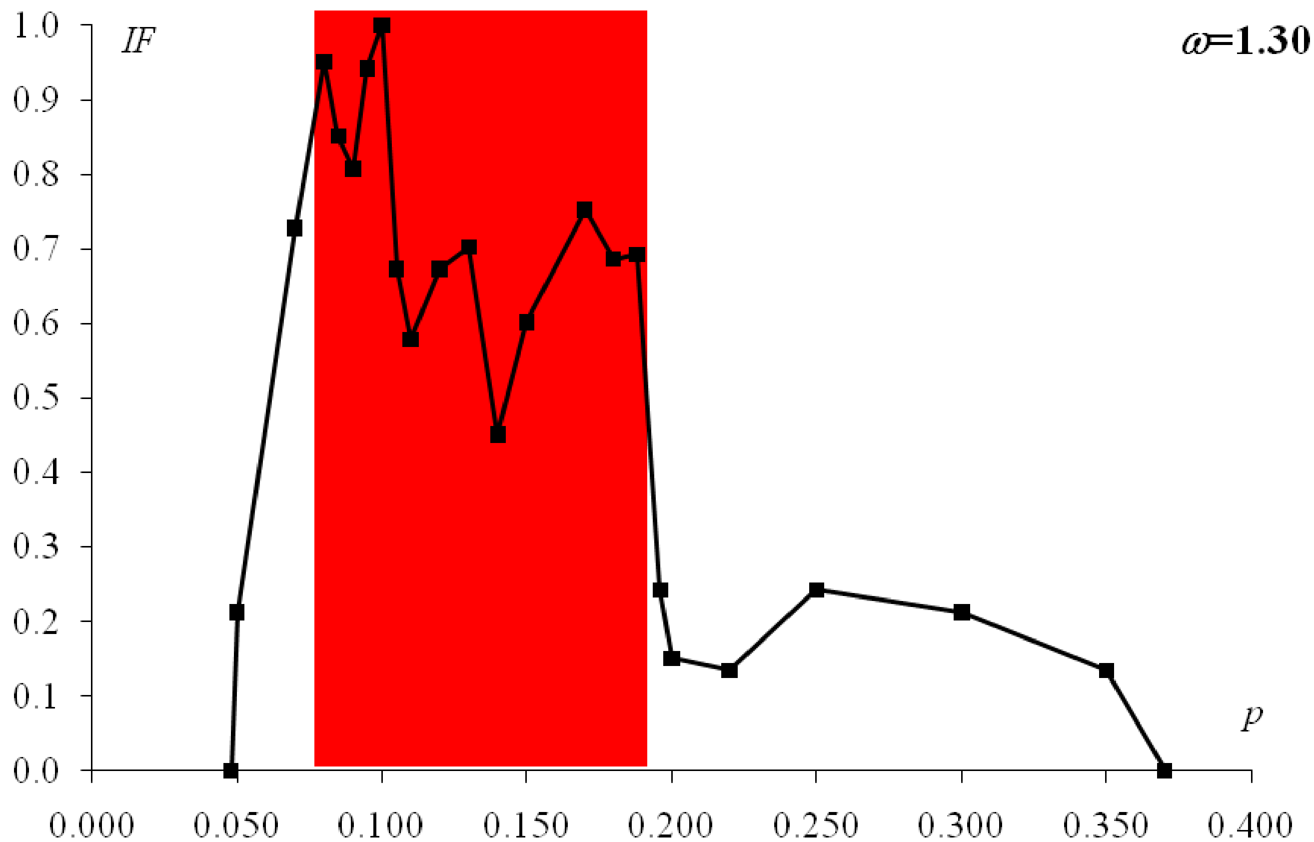

- Rotations are **robust** **only in the central part**: that is why they are **experimentally observed only there**!

Different ωs, same conclusions

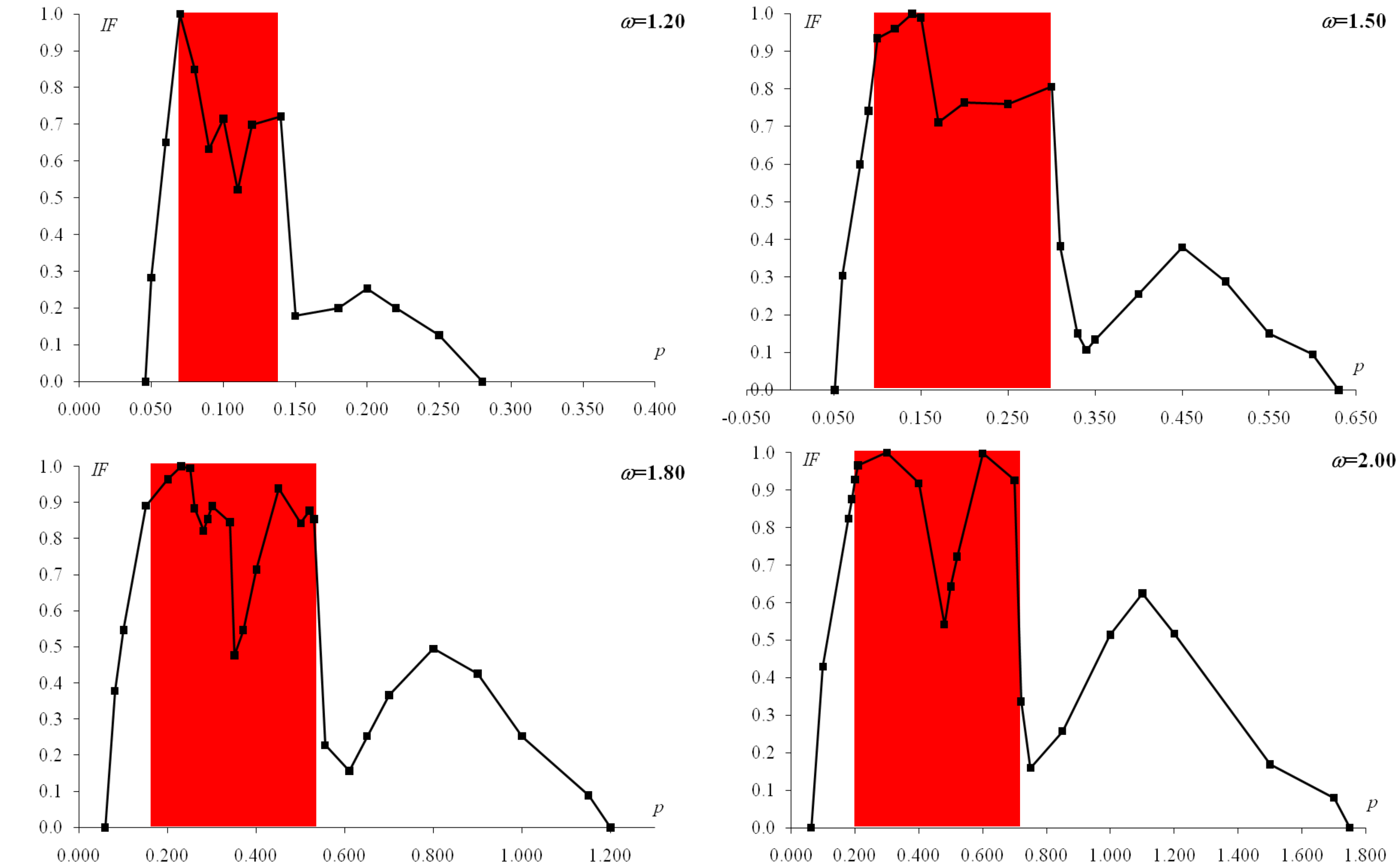

Different normalization for IF

The justification holds over the whole (p,ω) parameters space

Integrity by increasing ω

- Basins of attraction for low frequencies are smaller than those for high frequencies

ω=1.2, p=0.07

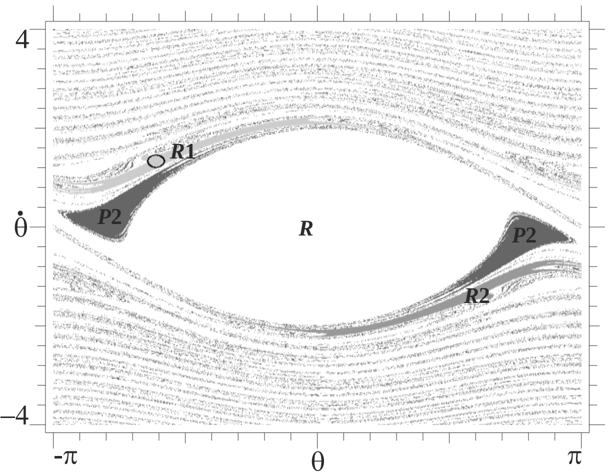

ω=1.8, p=0.23

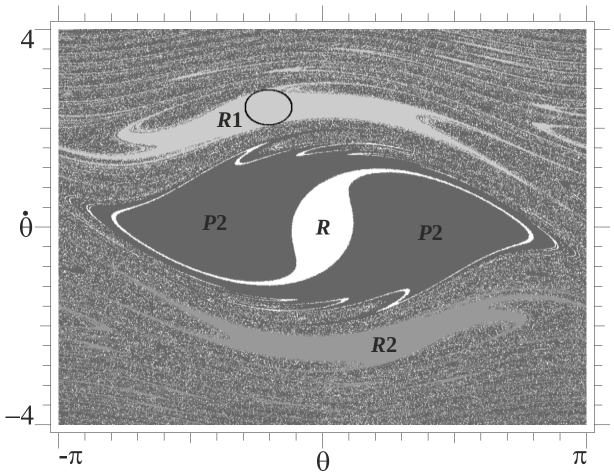

ω=2.2, p=0.30

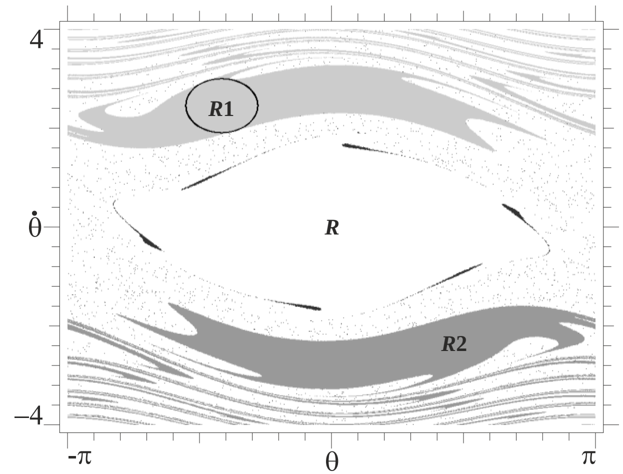

- Usefulness of high excitation frequencies to have rotations (for energy production)

The surface IF(p,ω)

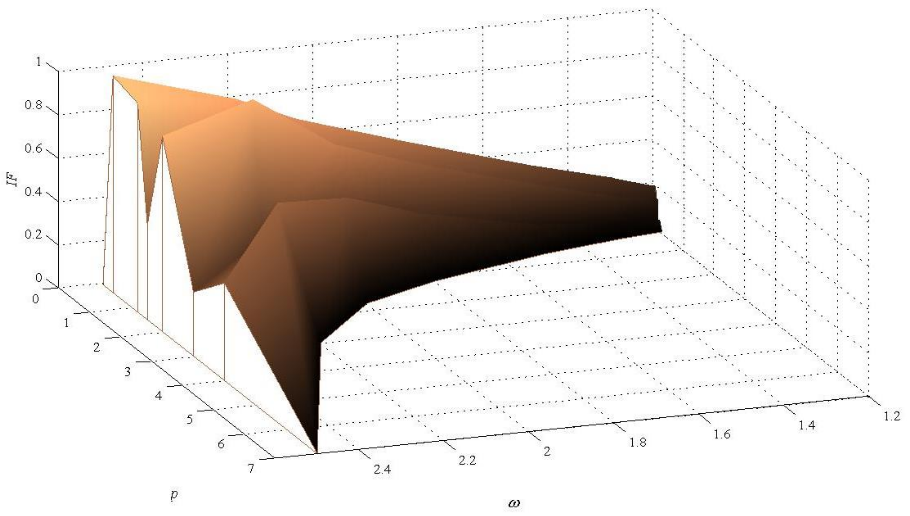

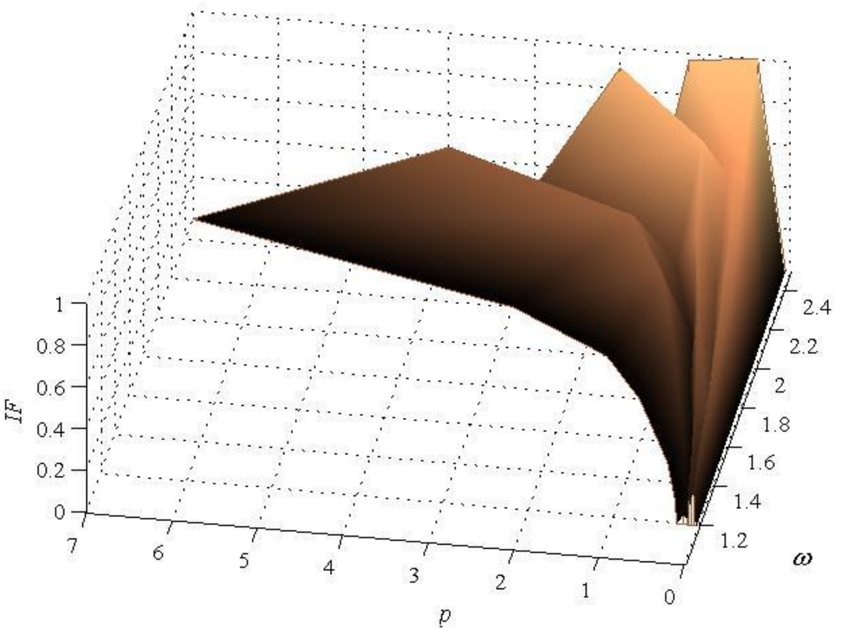

- Same normalization of IF → comparable results
- Confirmed that integrity increases for increasing excitation frequencies
- A number of ridges for increasing excitation amplitudes

Comparison of numerical and experimental results (1)

- Contour plot of IF(p,ω) vs experimental results

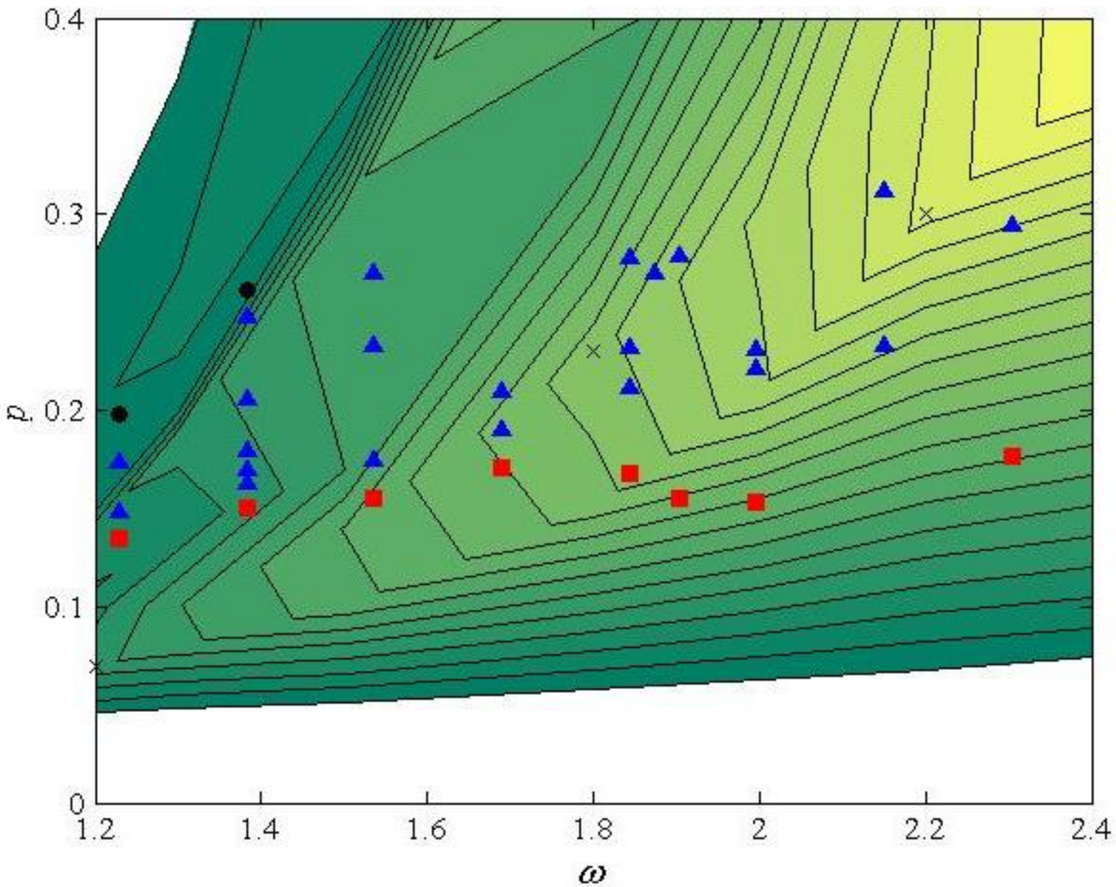

For ω<1.6 experim. points are on the 'plateau' of high *IF*

The *PD* points are after the sudden fall of *IF*, which can be considered, as the "experimental PD threshold"

Comparison of numerical and experimental results (1)

- Contour plot of IF(p,ω) vs experimental results

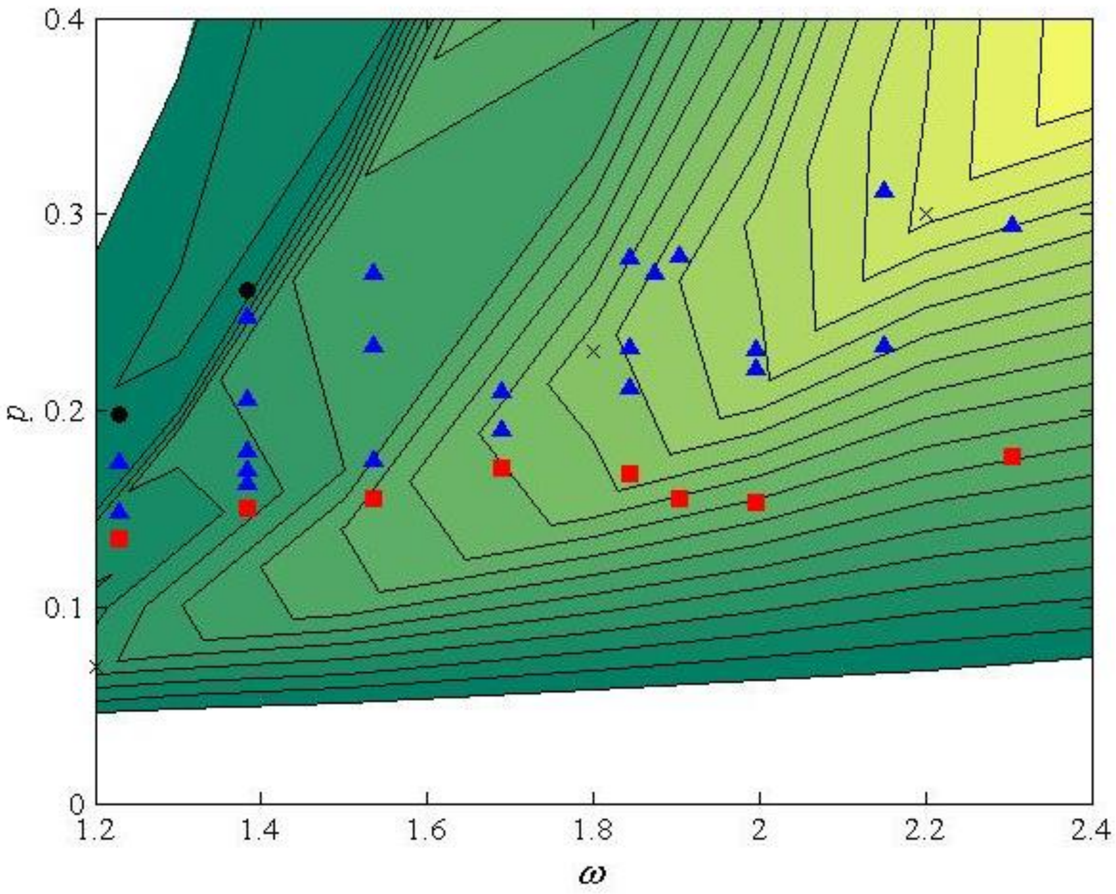

The bottom curve p_{SN}^{exp} follows the minor fall after the first peak of the IF

The fact that it is not below is likely due to experimental approximations (e.g. non perfect control on the i.c.)

Comparison of numerical and experimental results (1)

- Contour plot of IF(p,ω) vs experimental results

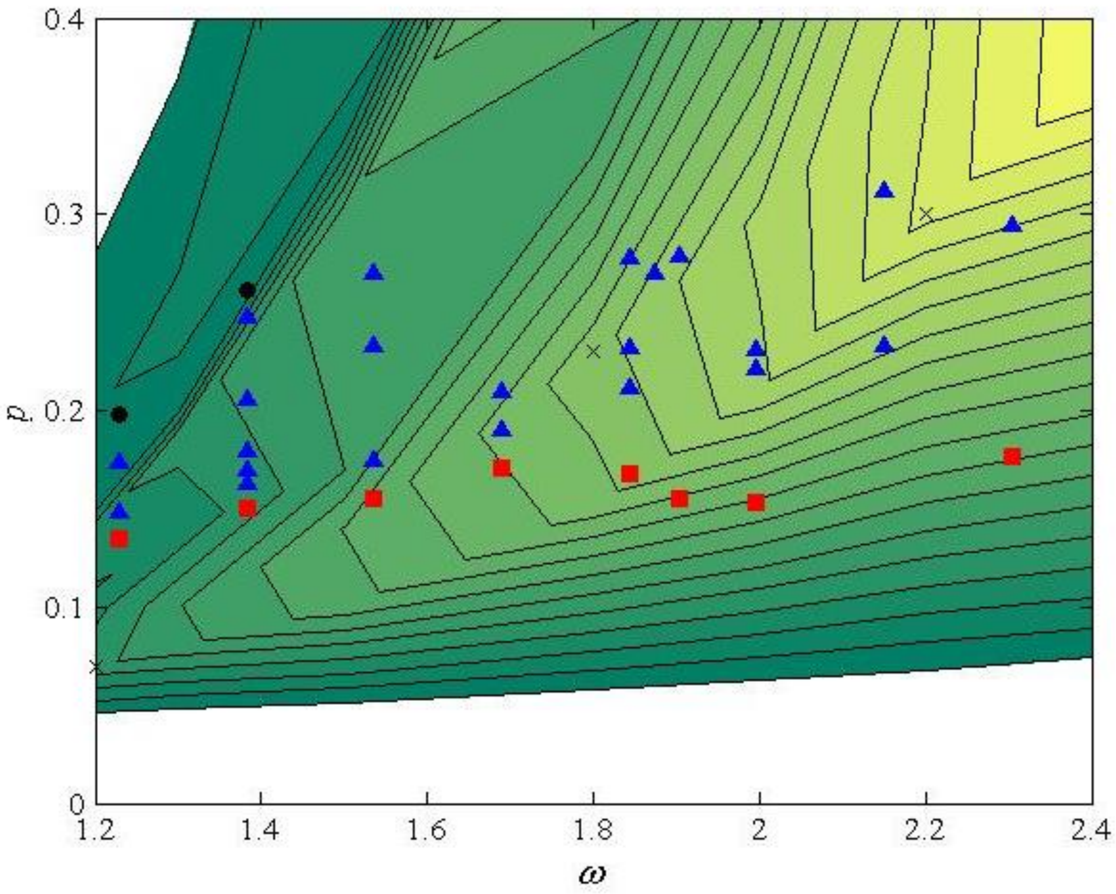

For ω>1.6 experim. points are around the main ridge of the *IF*

Definitive confirmation that only rotations with large robustness and dynamical integrity can be practically observed

Comparison of numerical and experimental results (1)

- Contour plot of IF(p,ω) vs experimental results

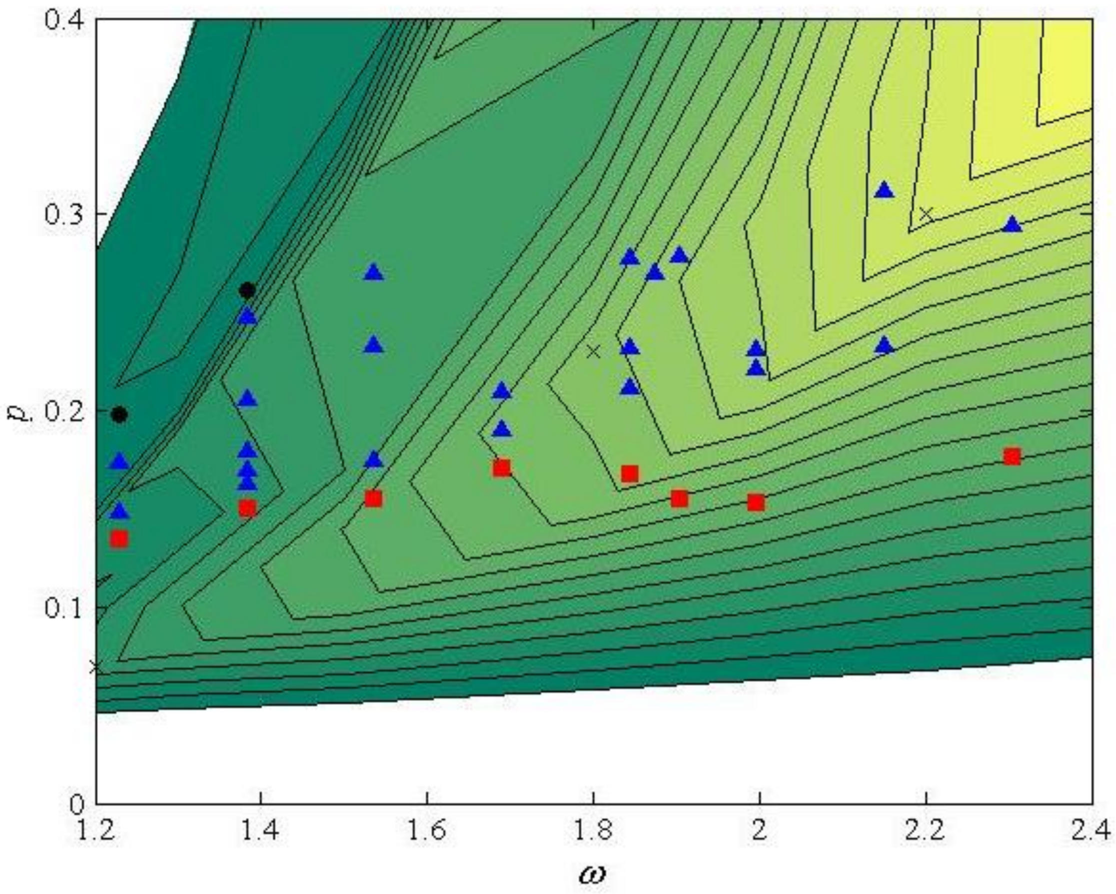

For ω>2.2 we cannot further increase the amplitude of the wave at generator

The bottom curve p_{SN}^{exp} is now on a level curve of IF (showing the minimal dynamical integrity necessary for the onset of experimental rotations)

MEMS: experimental system and model

Experiment

lower electrode
(sylicon substrate)

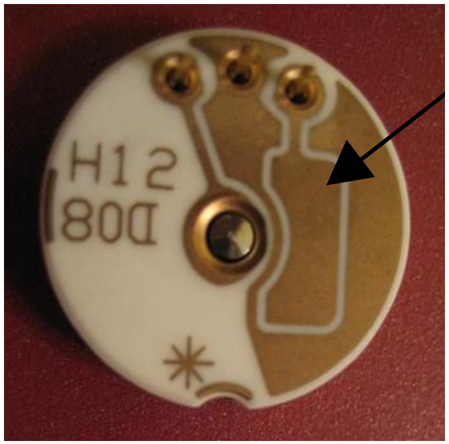

upper electrode
(proof mass)

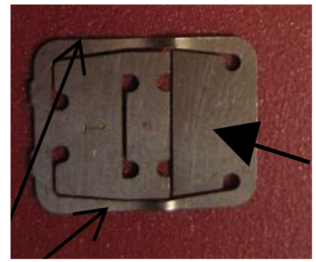

cantilever beams

capacitive
accelerometer

The proof mass is suspended over the substrate by the two cantilever beams.

Lower electrode provides electrostatic and electrodynamic excitation which entails oscillation of the proof mass in the out-of-plane direction (out of the substrate plane)

s.d.o.f.
model

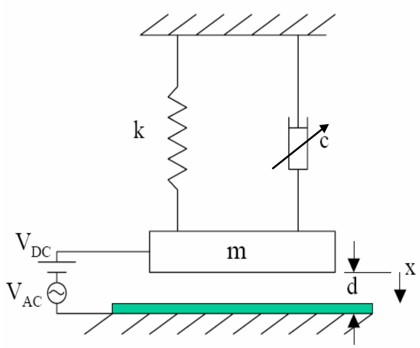

- lumped mass → proof mass
- spring → two cantilever beams

$$m\ddot{x} + c(x)\dot{x} + kx = \frac{\varepsilon A[V_{DC} + V_{AC}\cos(\Omega t)]^2}{2(d-x)^2}$$

Experimental set-up

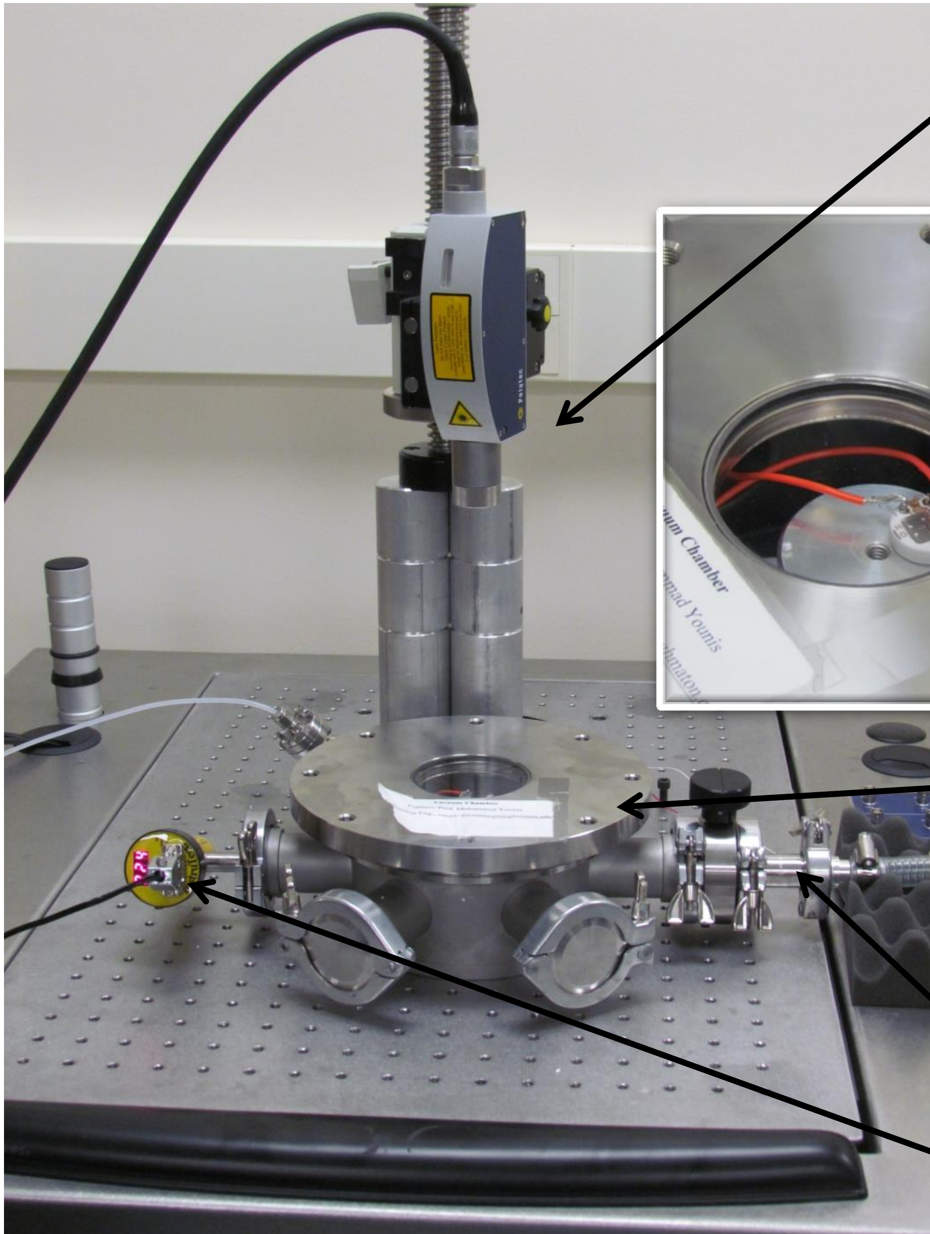

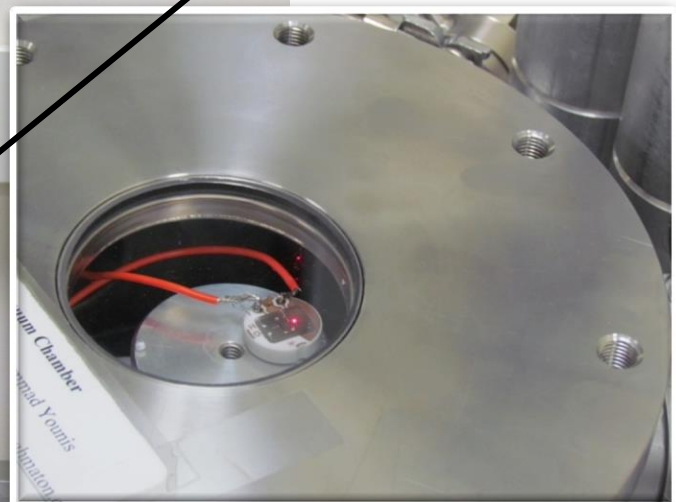

Laser doppler vibrometer

The device is mounted inside the vacuum chamber

Vacuum chamber

The device is placed inside the chamber, underneath the laser

Pressure gauge

Electrical connection

Resonance

$V_{DC} = 40.1\ Volt$ and $V_{AC} = 18.4\ Volt$

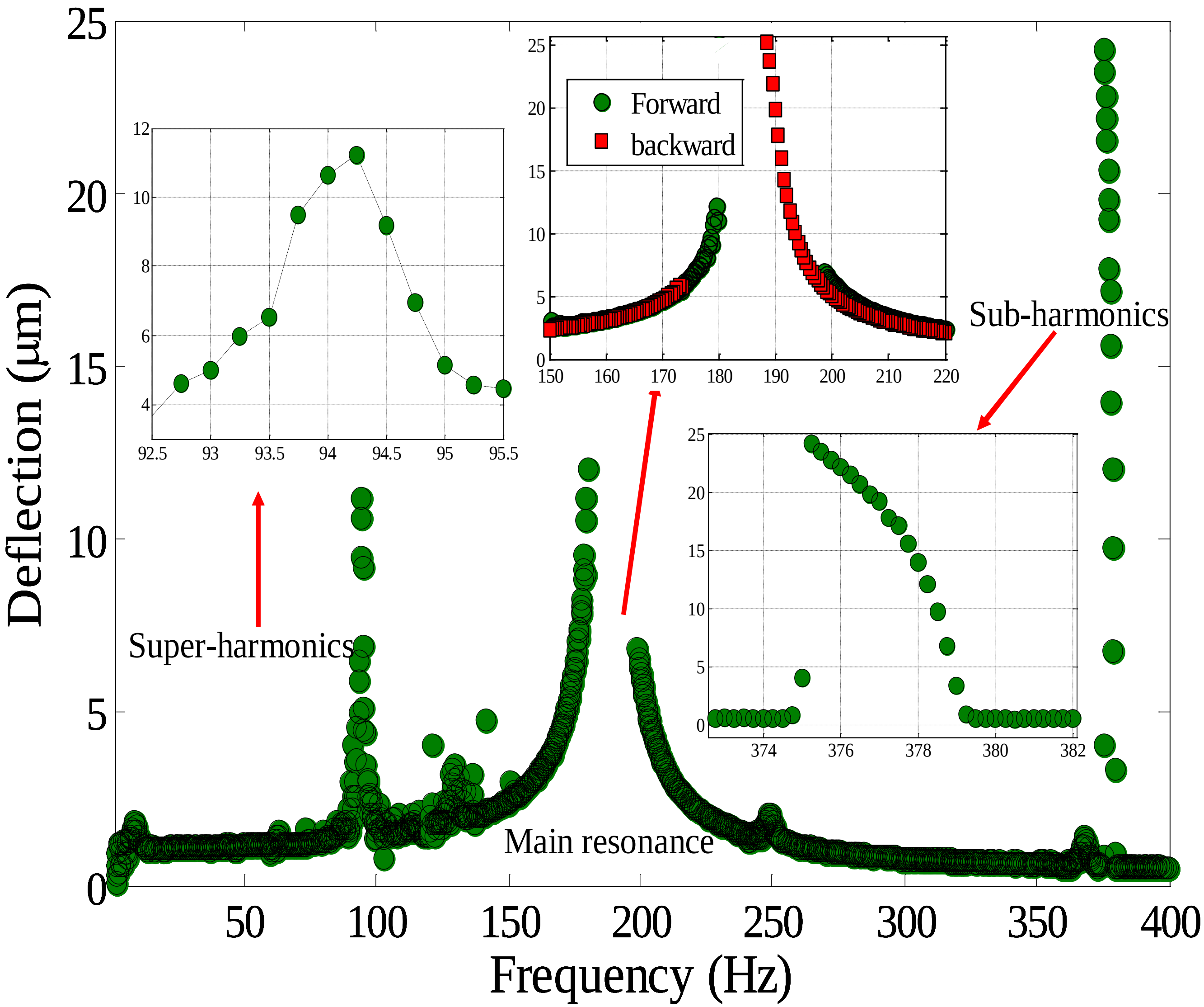

Frequency response (1)

V_{AC} = 32.4 V

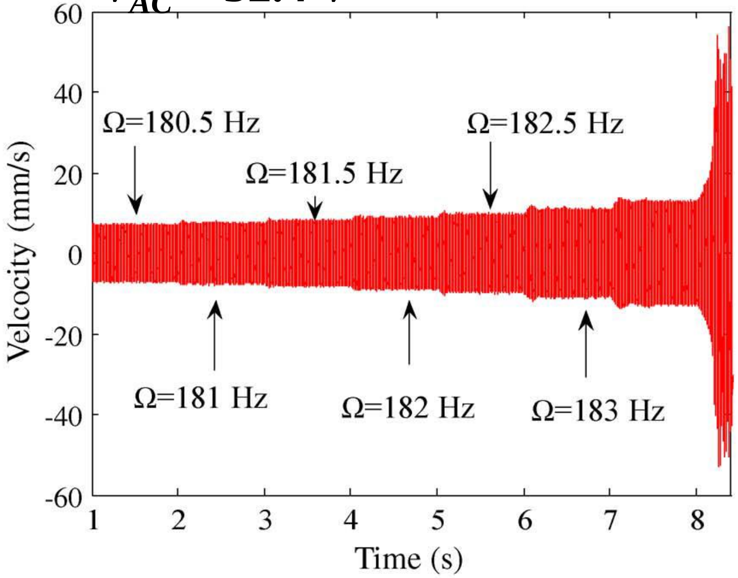

V_{AC} = 32.4 V

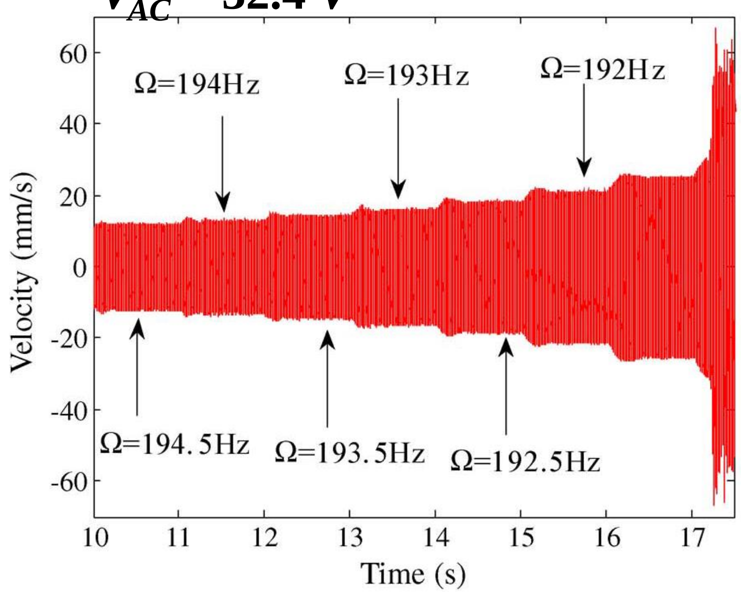

Experimental time histories in a neighborhood of *primary resonance*

***forward* sweep**

when the attractor disappears, the device directly undergoes *dynamic pull-in*

***backward* sweep**

Operatively:

- **dynamic voltage is kept constant**
- **frequency is varied slowly, i.e. *quasi-statically***

Frequency response (2)

Collecting information from many time histories, **frequency-response curves** describing the experimental outcome are built

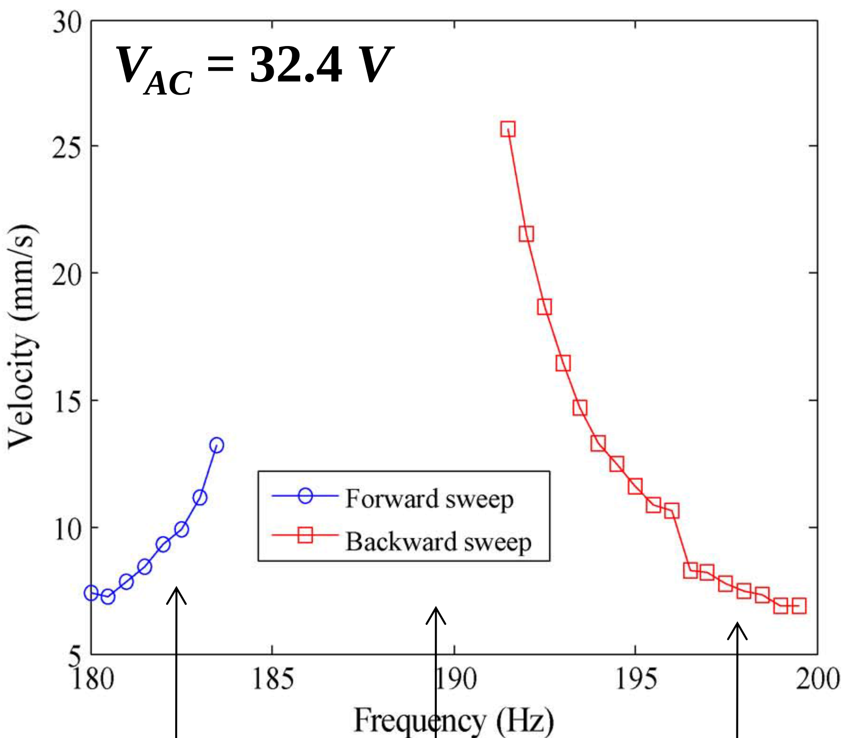

nonresonant branch

resonant branch

dynamic pull-in

- Many frequency sweeps, at different V_{AC} values, provide a ***complete*** description of the dynamics
- To compare the sweeps among them, they are acquired by adopting the "*same*" experimental conditions:
  - $V_{DC} = 0.7\ V$,
  - pressure: 153 mtorr,
  - frequency step: 0.5 Hz

Frequency response (3)

Collecting the values of (V_{AC}, Ω) where ***each attractor experimentally disappears***, we can draw the experimental **behavior chart**, which illustrates the **experimental pull-in bands**

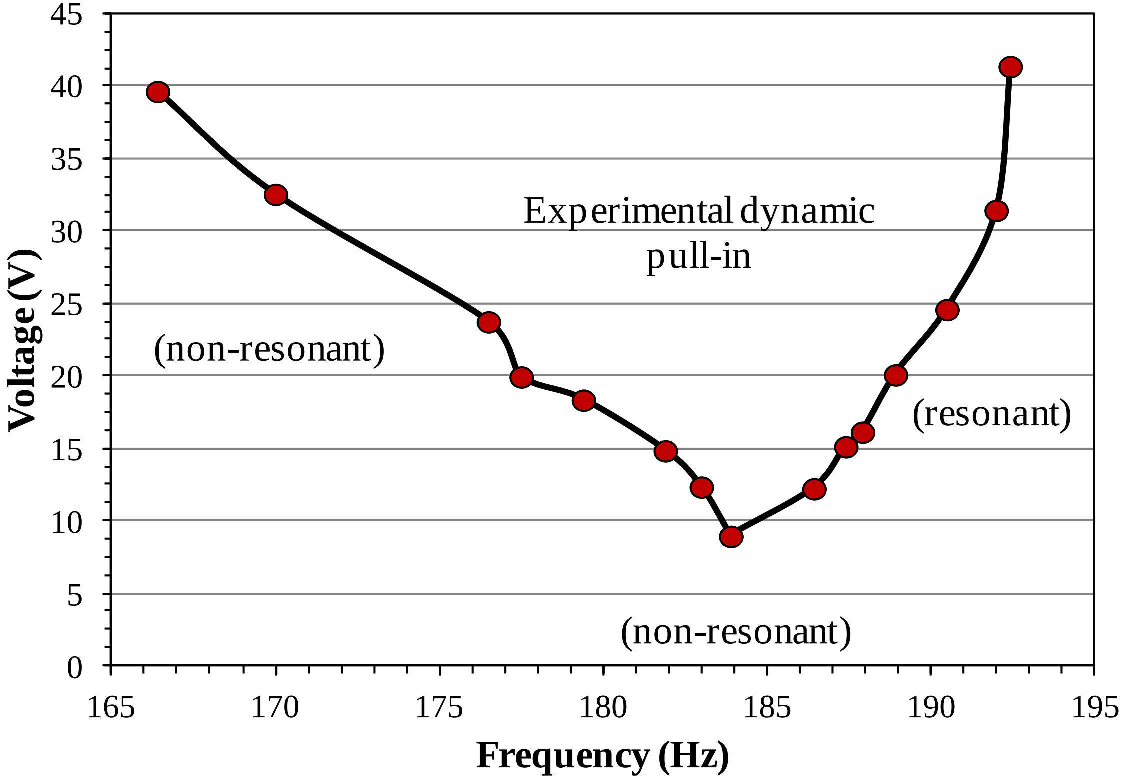

Unknown model parameters to be characterized for obtaining an *applicable confident estimate* of the MEMS response, with its experimental bands, up to high V_{AC} voltages

Model characterization (1)

We extract the ***unknown parameters*** from direct measurements and from static and dynamic tests

1) ***Stiffness coefficient***

This is extracted by focusing on the static bifurcation diagram and by **matching the experimental data with the theoretical predictions**

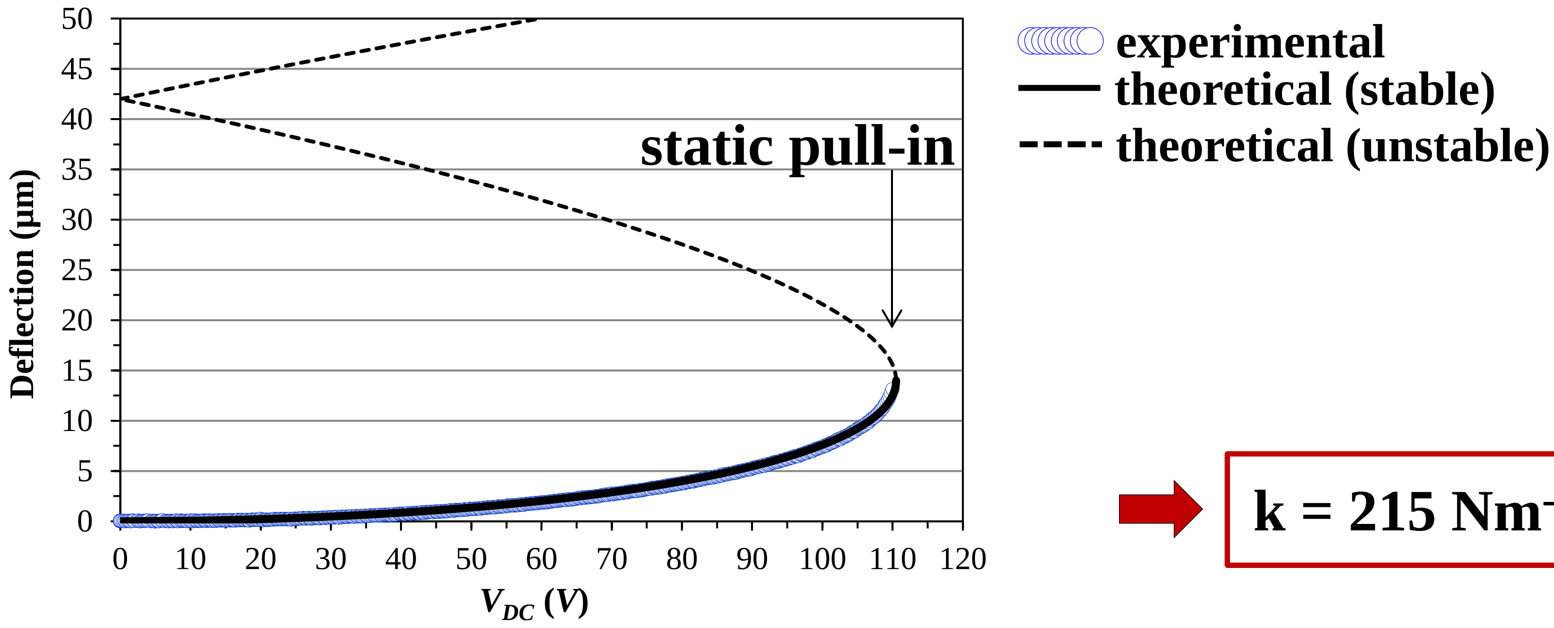

$k = 215\ Nm^{-1}$

Model characterization (2)

2) ***Effective mass of the proof mass***

This is extracted by **matching the experimental natural frequency**

natural frequency
$\Omega = 192.5$ Hz

$\boxed{\boldsymbol{m = 0.14697 \text{ g}}}$

3) ***Damping coefficient***

We consider the viscous squeeze-film damping contribution, since is the main source of energy loss in the analyzed MEMS.

We resort to the Blech model [Younis, 2011], which analytically solves the linearized Reynolds equation:

$$c(x) = \frac{768\eta_{eff} PaA^2}{\pi^6 (d-x)^3} \left(\frac{2}{[4+\sigma(x)^2/\pi^4]} \right) \qquad \text{with:} \qquad \sigma(x) = \frac{12A\Omega\eta_{eff}}{Pa(d-x)^2}$$

- pressure: 153 mtorr
- assuming a constant gap between the electrodes

$\boxed{\boldsymbol{c = 1.48 \text{ g/s}}}$

Governing equation

The **governing equation of the MEMS device** becomes:

$$\boxed{\ddot{x} + 10.1\dot{x} + 1.4629 \cdot 10^{6} x = 1.2 \cdot 10^{-12} \cdot \frac{[40.1 + V_{AC} \cos(\Omega t)]^{2}}{(42 \cdot 10^{-6} - x)^{2}}}$$

which is the equation used for the forthcoming simulations

Mathematical properties of the model

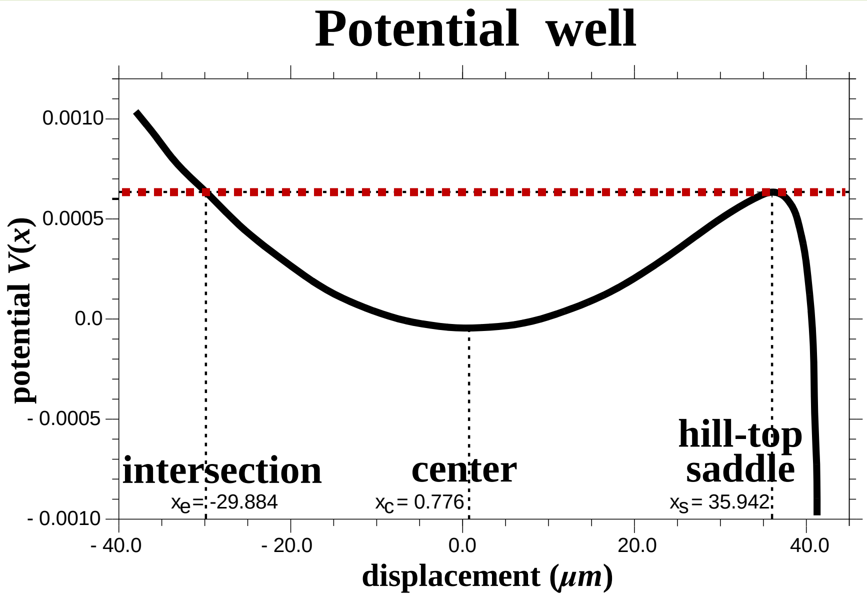

The unforced, undamped system is Hamiltonian with a **single asymmetric** potential well, of **softening** type, with **escape** direction

$$V(x) = k\frac{x^2}{2} - \frac{\varepsilon A V_{DC}^2}{2(d-x)}$$

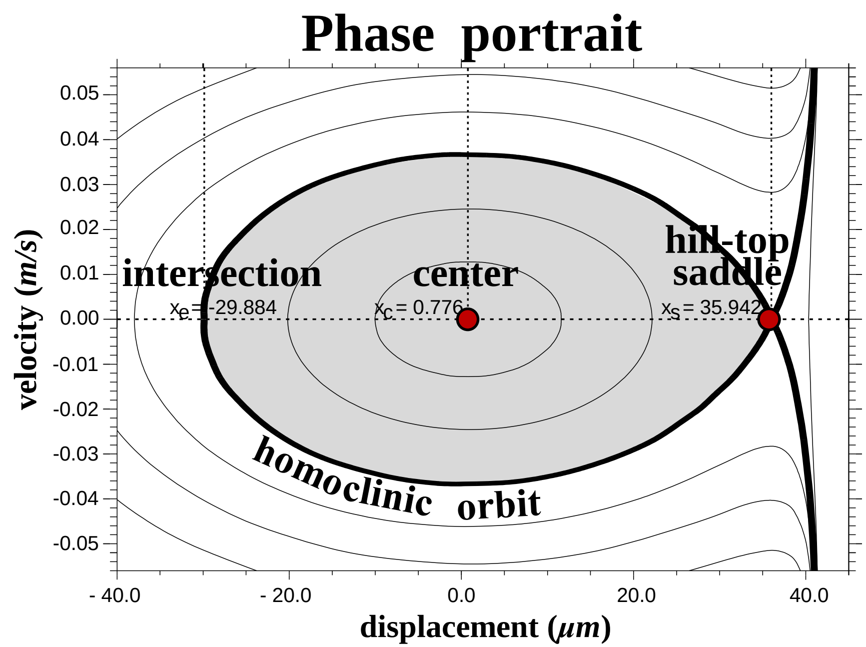

- Two equilibrium points: a ***center*** and a ***hilltop saddle***
- Stable and unstable manifolds of the hilltop saddle coincide
- ***Homoclinic orbit*** separating in-well oscillations and out-of-well escape

Device vs model response (1)

The model properly represents all the ***main features*** of the **experimental data**

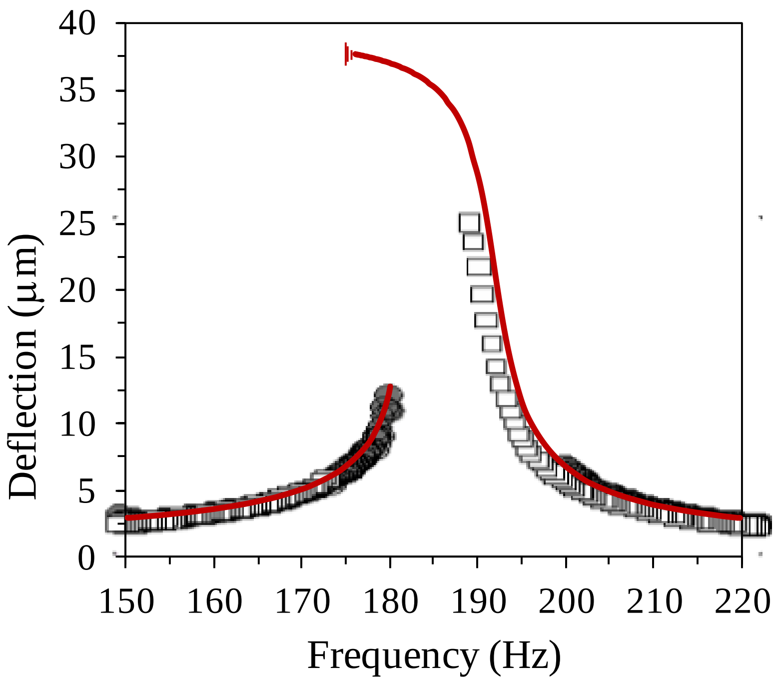

- value of natural ***frequency***
- ***softening*** behavior in its neighborhood, with the characteristic bending toward lower frequencies
- ***separation*** width ***between resonant and nonresonant branches***

The concurrence of results confirms our ***confidence in the model***, which, despite the apparent ***simplicity***, is able to catch all the main nonlinear phenomena

Device vs model response (2)

But, despite the good matching, the ***range of existence*** of each attractor is **smaller in practice than in the theoretical simulations**

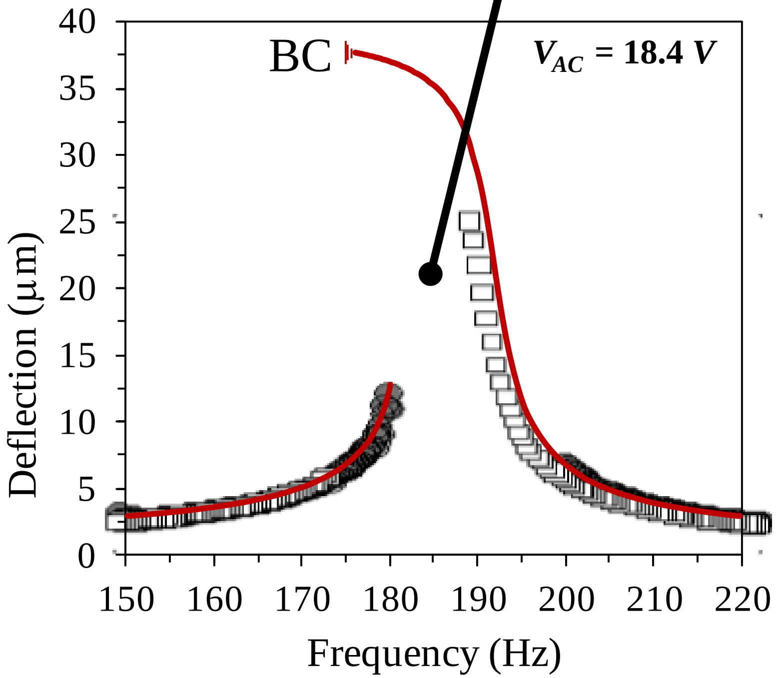

Resonant branch, decreasing frequency:

- ***Theoretical model*:** the attractor experiences the classical period-doubling (PD), followed by chaotic motion and *boundary crisis* (BC).
- ***Experimental data*:** the attractor **does not exhibit the *last part* of the theoretical branch**

Similar behavior in the ***nonresonant branch***

Each branch **disappears *in practice*** where each **attractor is *theoretically* expected to exist**

Device vs model response (3)

- Thus, **experimental data** have an **intermediate interval without bounded solutions**, where the **escape** is **inevitable**, because there are **no other attractors**

- This outcome **does not occur** in the **theoretical simulations** at the same V_{AC}, where, on the contrary, all ranges exhibit **at least one attractor** (moreover, there is a small range of coexistence of both branches)

The **inevitable escape** region appears also in the **theoretical curves** but only at ***larger*** $\boldsymbol{V_{AC}}$ **excitations**

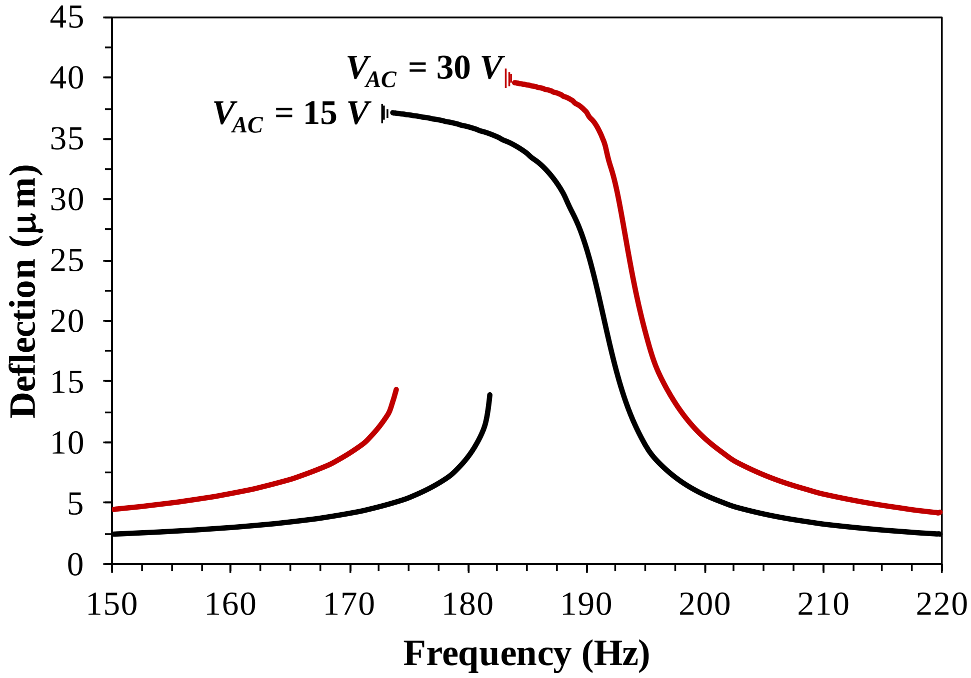

Theoretical vs experimental escape (1)

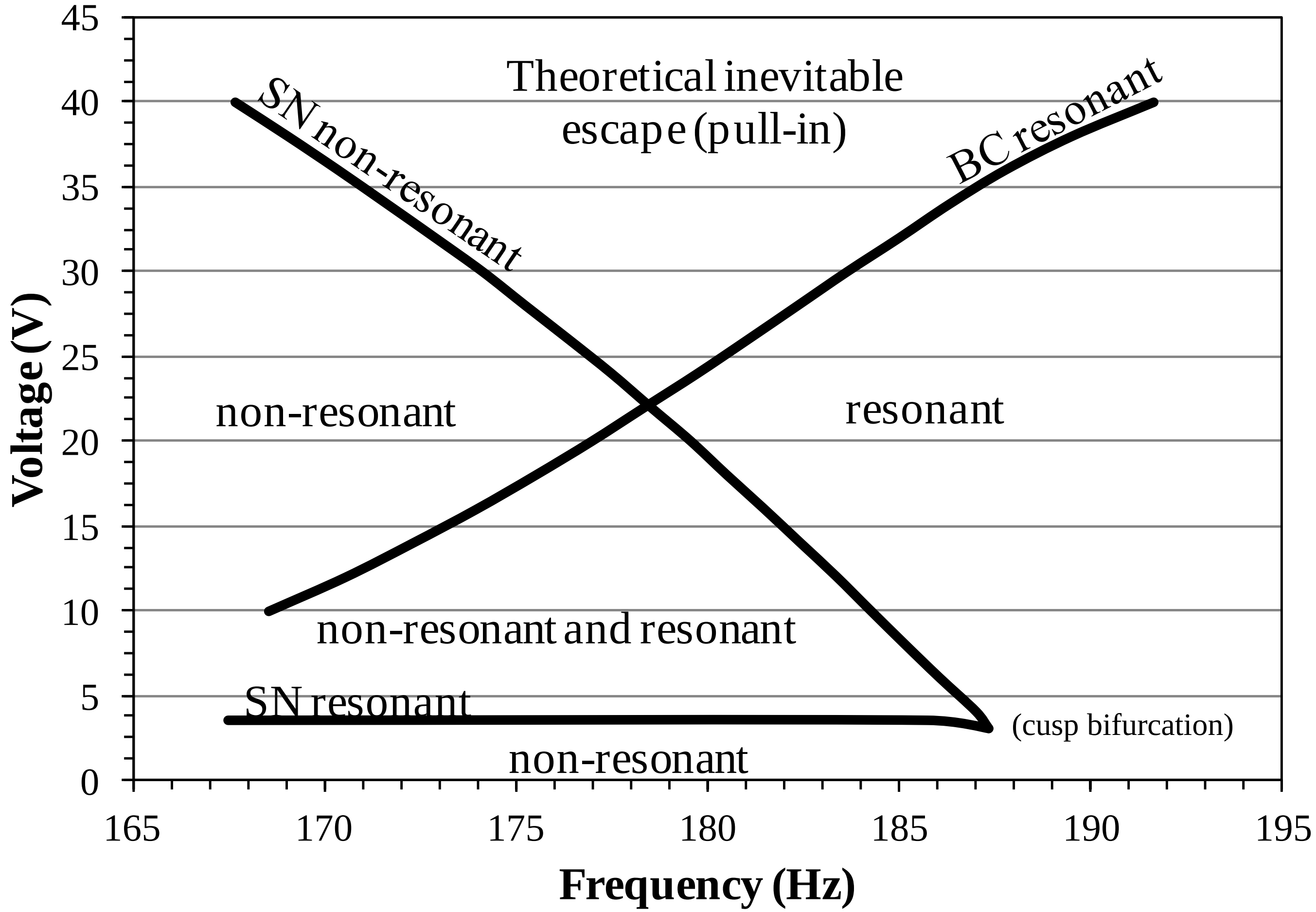

The ***behavior chart*** with the thresholds of ***theoretical*** appearance and/or disappearance of each attractors shows the **theoretical bounds of existence** of each branch

Theoretical vs experimental escape (2)

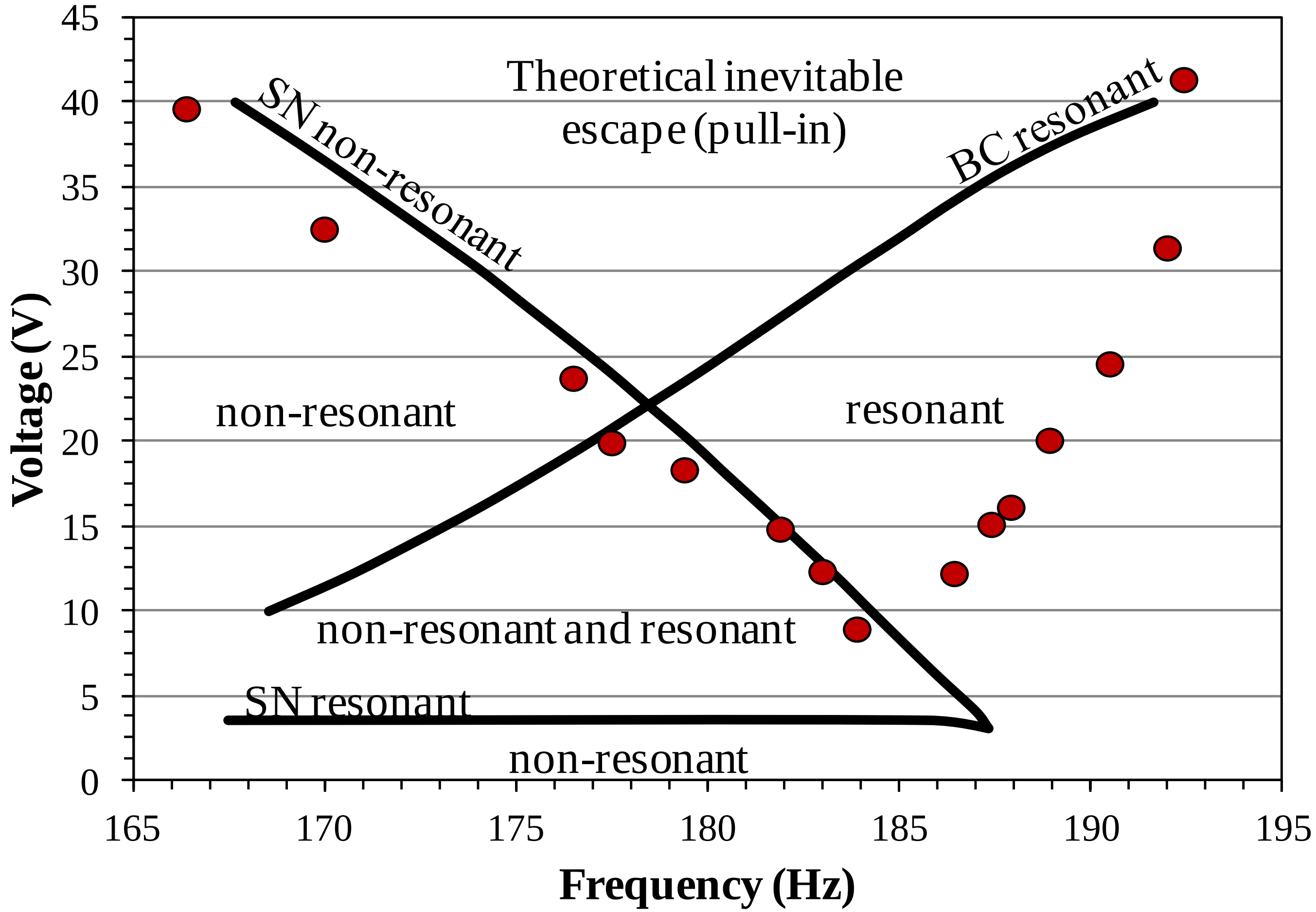

Theoretical pull-in (inevitable escape), bounded by SN and BC, **is systematically above** the **experimental pull-in threshold**

How to justify this experimental evidence? By ***dynamical integrity***

Theoretical vs experimental escape (3)

disturbances commonly encountered in practice produce uncertainties in operating initial conditions

(discontinuous steps in the frequency sweeps, approximations in the model, in damping, in identifying the unknown parameters)

existence and stability of attractor do **NOT consider the inevitable presence of *disturbances*:**

do NOT mean 'safety' from dynamic pull-in

DYNAMICAL INTEGRITY is the aspect of **global analysis** which illustrates if an **attractor is sufficiently robust to DISTURBANCES** i.e. paralleled by a **sufficiently robust SAFE BASIN**

Attractors and basins (1)

Global dynamics: **topology of the basins** and its **modifications by varying parameters**

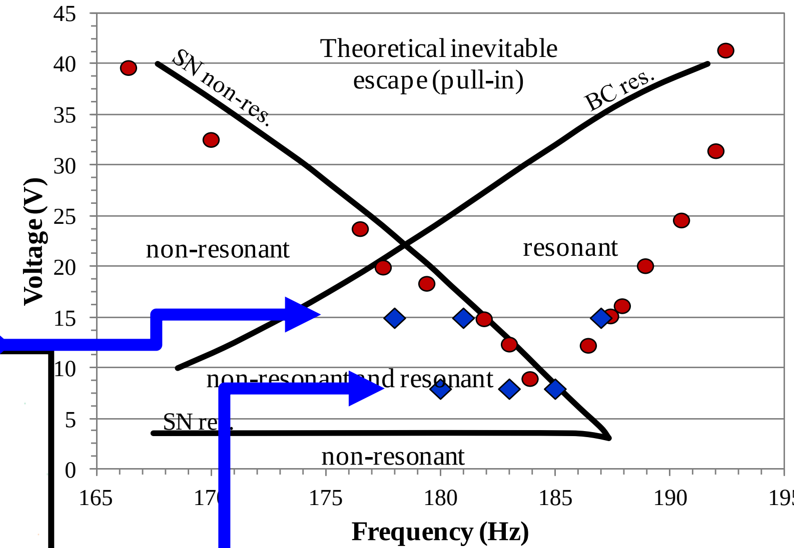

V_{AC} **= 15 *V***

increasing Ω

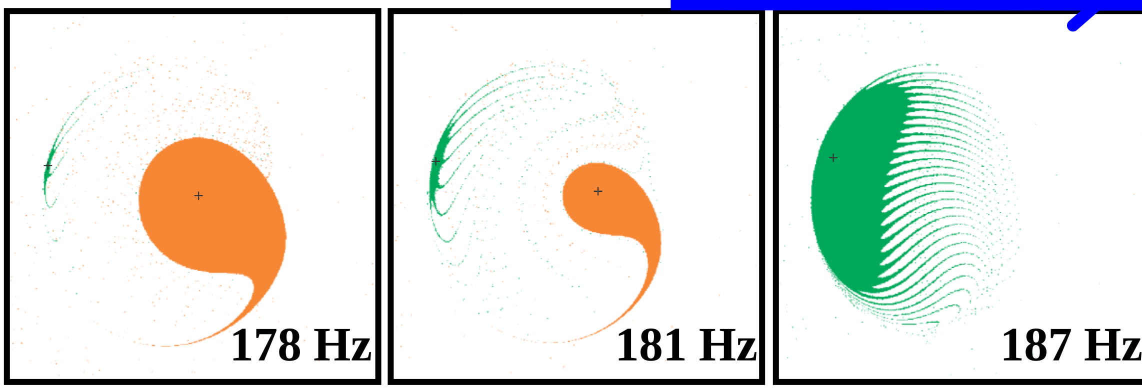

V_{AC} **= 8 *V***

increasing Ω

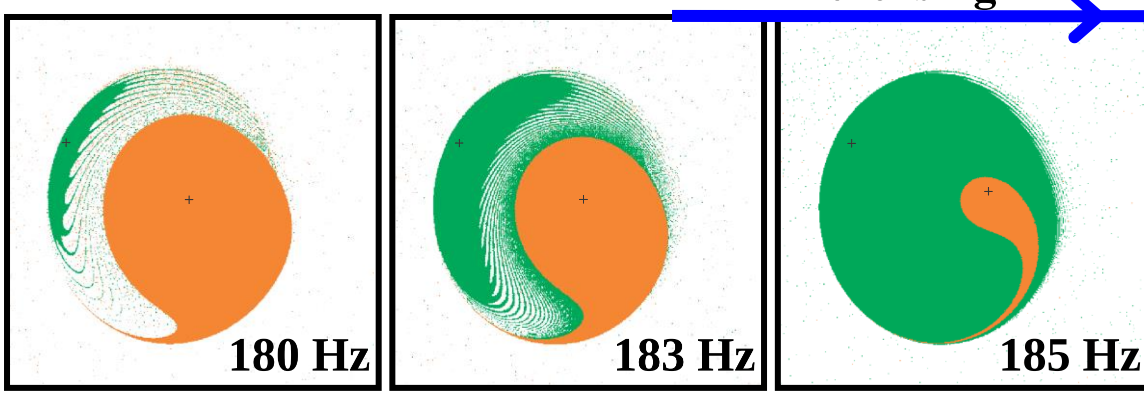

Erosion much more evident !

fractal (white) tongues of escape **separate** the basins of the resonant and non-resonant branch and **shrink** them

Attractors and basins (3)

The *experimental* disappearance of each attractor occurs exactly when the *compact area* of its basin becomes too much reduced

V_{AC} = 20 V

increasing Ω

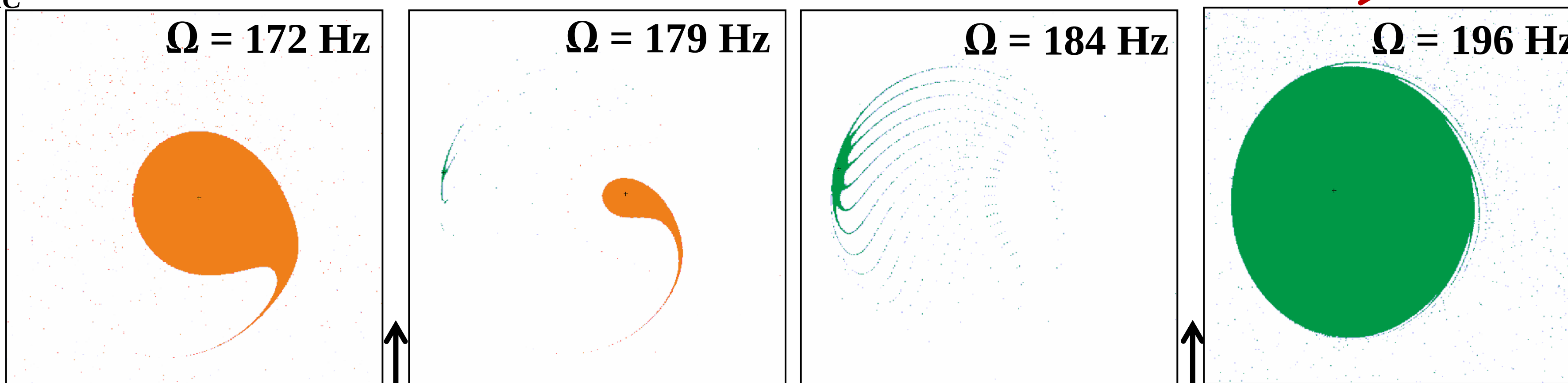

ONLY NON-RESONANT

ONLY RESONANT

EXPERIMENTAL DISAPPEARANCE OF NON-RESONANT
Ω = 177.5 Hz

EXPERIMENTAL DISAPPEARANCE OF RESONANT
Ω = 188.9 Hz

EXPERIMENTAL DYNAMIC PULL-IN
Ω = [177.5; 188.9] Hz

non-resonant

resonant

Tools of analysis

Analyze the disappearance of each attractor to detect the parameter ranges where it may *practically* (and not theorically) vanish

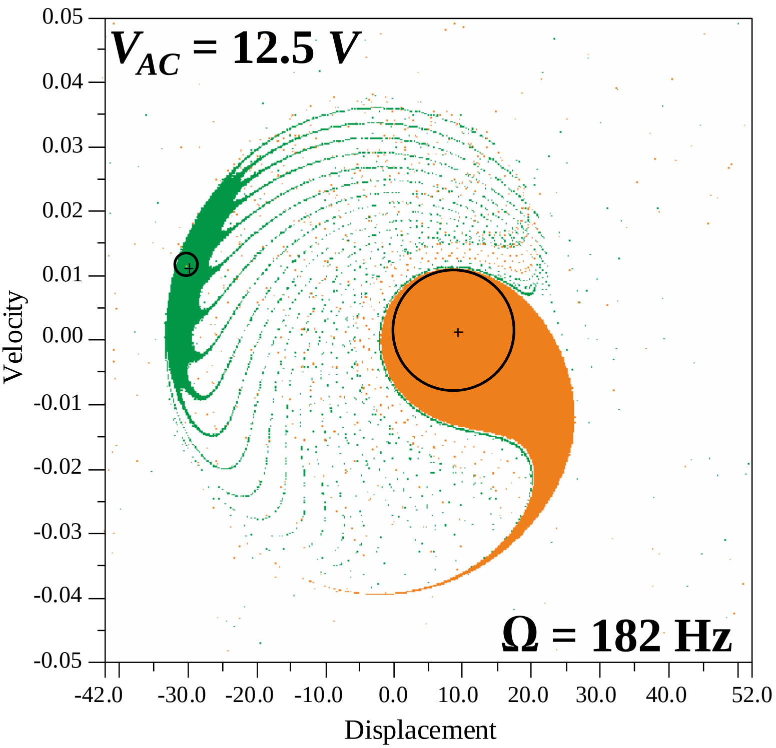

Safe basin: the own basin of attraction of each attractor

- safe condition: having, at the steady-state dynamics, the motion under consideration
- unsafe condition: having other motions (bounded oscillations or escape)

Integrity measure: Local Integrity Measure (LIM)

- radius of the largest circle entirely belonging to the safe basin and centered at the attractor
- LIM considers only the compact ‘core’ and rules out the non-compact regions

Integrity profile (1)

Draw the integrity profiles describing the ***loss of dynamical integrity*** **(LIM)** when the frequency is varying

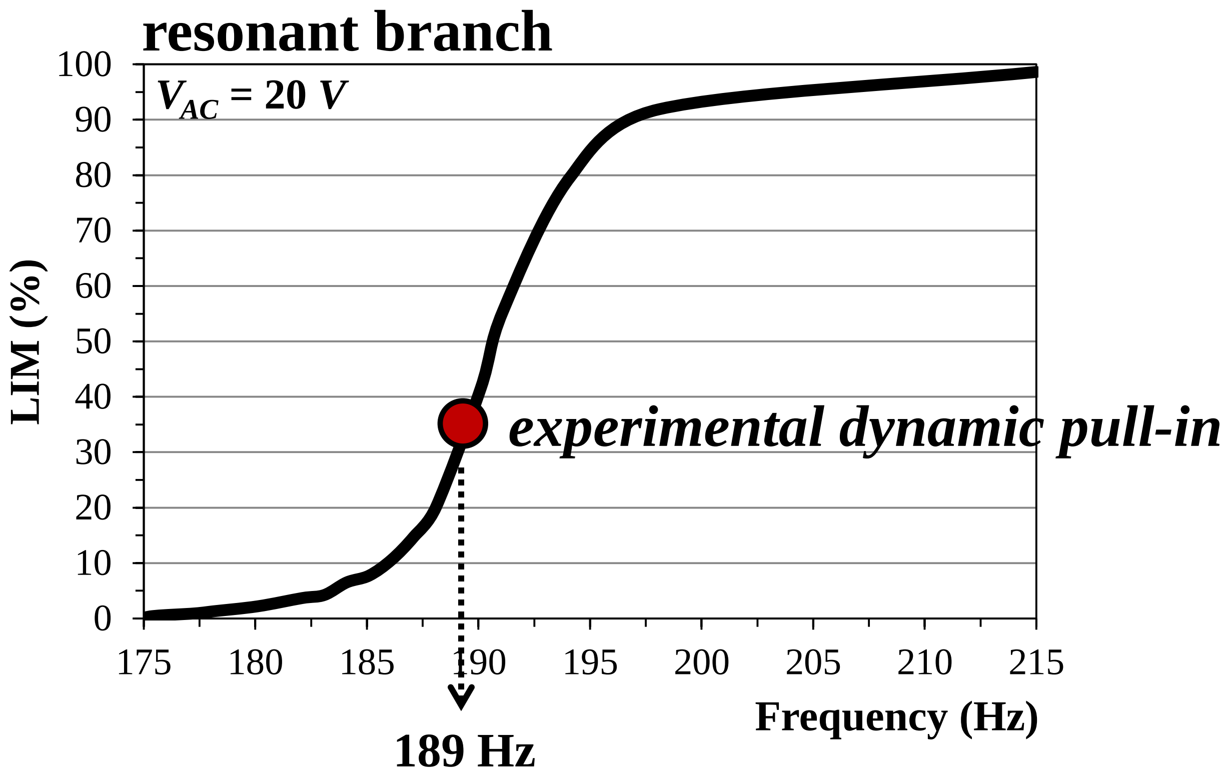

The smaller integrity enhances the ***sensitivity*** of the system to disturbances, and makes the attractor ***vulnerable*** **(it may disappear)**

Integrity profile (2)

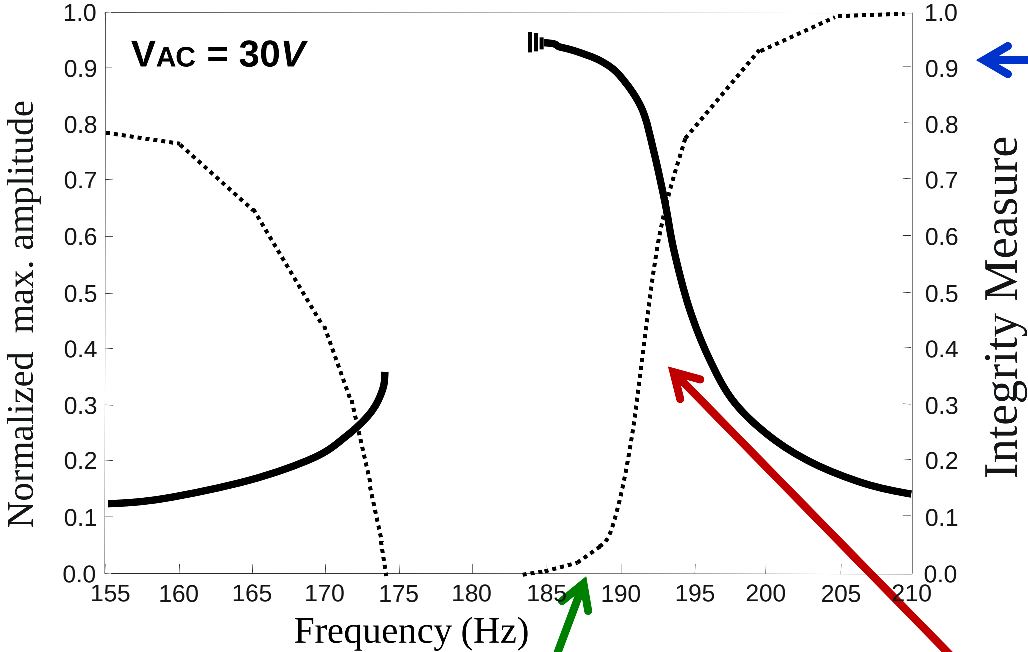

- **erosion** of safe basin is ***slow***
- only ***slight*** **decrement** of **IM**
- ***safe*** **small oscillations**

- ***very small*** **safe basin**
- ***cannot be caught*** by the sweeps
- happens together with very ***high*** **amplitude of oscillations**, ending with PD and chaotic motion

- **erosion** is very ***fast***
- appears together with **increasing** ***amplitude*** of oscillations
- ***experimental pull-in*** occurs **in this range** (LIM = 30%- 50%)

From *many* integrity profiles…

Integrity chart (1)

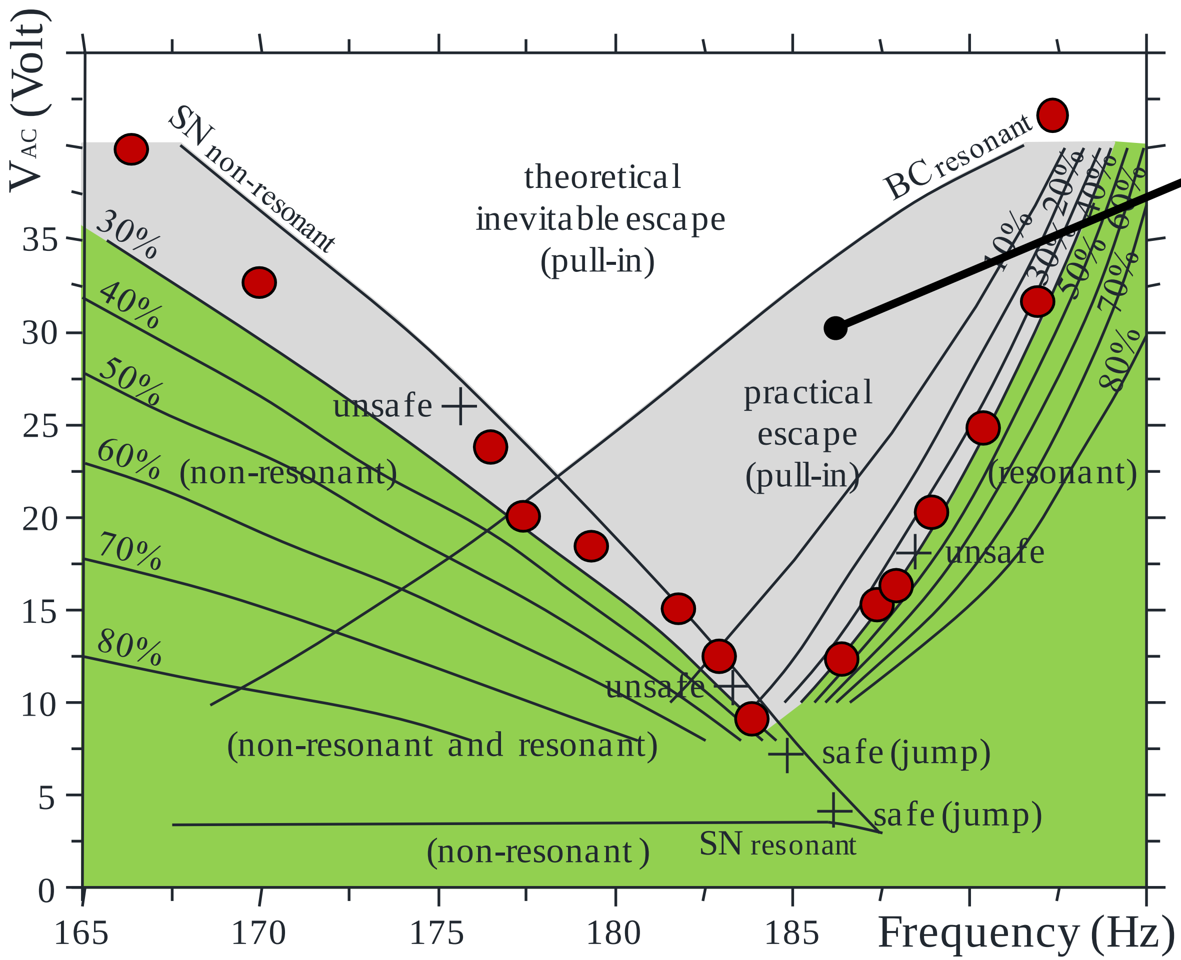

strong **discrepancy** between theory and experiments

experimental results theoretically *justified*

The experimental data follow 'exactly' the integrity curves

(curves of constant percentage of Integrity Measure, LIM)

Integrity chart (2)

We can identify:

- ***unsafe practical pull-in* threshold:**

  We can detect a **narrow range of LIM** where the **attractor experimentally vanishes (LIM=25-40%)**

- ***safe oscillations* threshold:**

  We can detect **a safe percentage,** above which the **device can be reliably operated (LIM=40%).**

  Below it, instead, (i.e. above the corresponding curve), **the device becomes practically vulnerable to pull-in**

The integrity curves successfully *interpret* and *predict* the experimental data, taking into account the inevitable existence of *disturbances*, which are unavoidable in practice

Guideline for design (1)

In addition, the **integrity chart provides a *complete* description of the expected final outcome, at *different* magnitudes of *disturbances***

***The integrity chart is a guideline for the design*:**

depending on expected disturbances,
it can be used to establish safety factors,
in order to operate the device in safe conditions,
according to the desired outcome

Guideline for design (2)

- **Pull-in practical threshold for:**

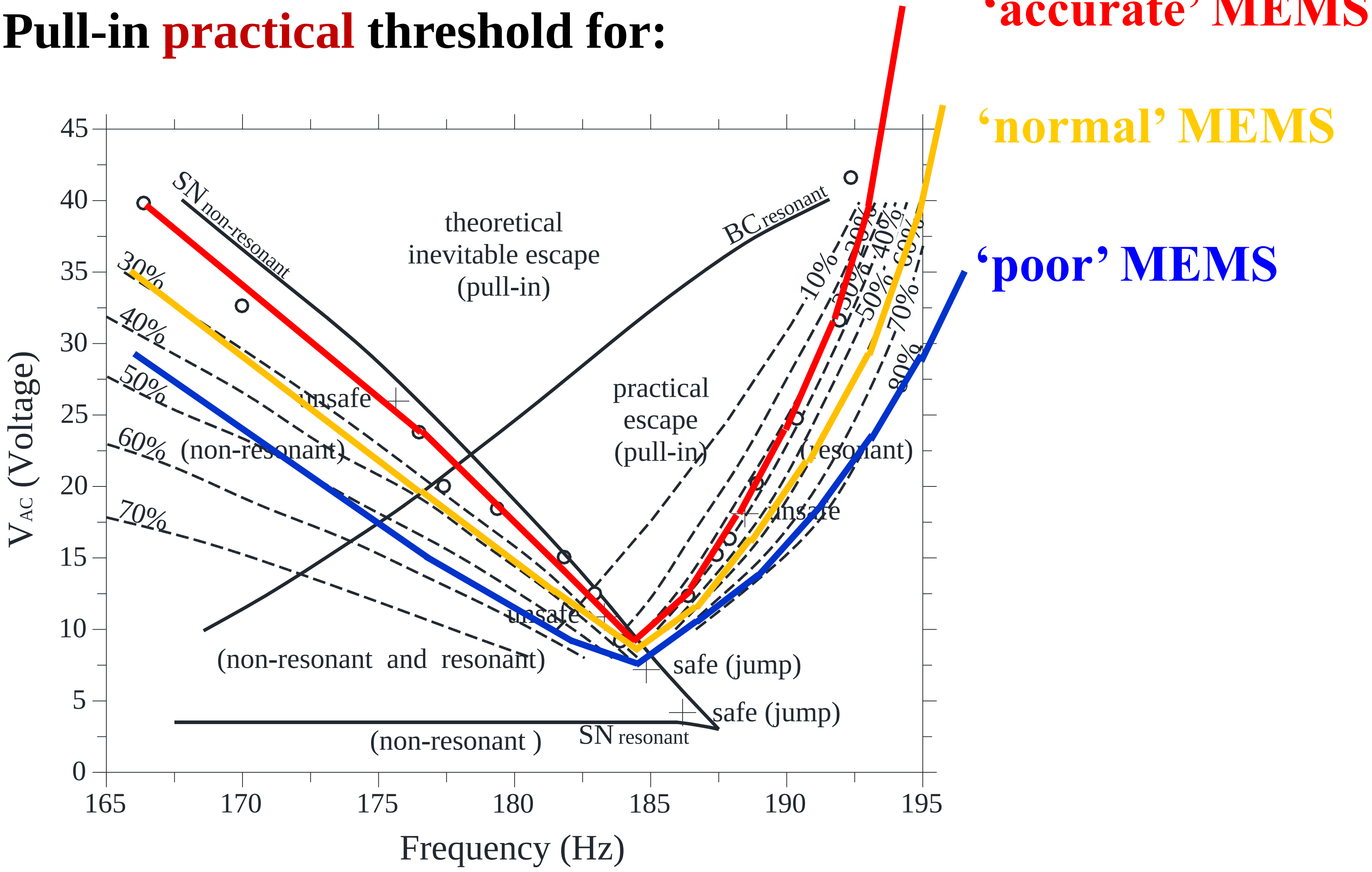

In summary (1)

<u>Classical analysis</u>

(local dynamics)

- **investigate appearance and/or disappearance (SN or BC) of each attractor**
- **behavior charts**

Inevitable escape (boundary crisis, saddle nodes) *does not predict* practical pull-in

<u>Dynamical integrity analysis</u>

(global dynamics)

- **attractor-basins phase portraits**
- **safe basin and integrity measure**
- **integrity profiles and integrity charts**

Curves of constant percentage of Integrity Measure *predict* experimental data

In summary (2)

The integrity chart summarizes the *overall scenario* of loss of *structural integrity*

- **<u>Integrity curves</u>**

  interpret the existence of disturbances existing in experiments and realistic conditions

- **<u>Curves of theoretical disappearance of attractors</u>**

  represent theoretical limit cases when disturbances are absent, which never occur in practice